EarthArXiv preprint of manuscript in press at *Geophysical Research Letters*
https://doi.org/10.1029/2020GL087669

River inflow dominates methane emissions in an Arctic coastal system

Cara C. Manning[1], Victoria L. Preston[2,3], Samantha F. Jones[4], Anna P. M. Michel[2], David P. Nicholson[5], Patrick J. Duke[4,†], Mohamed M. M. Ahmed[4], Kevin Manganini[2], Brent G.T. Else[4], and Philippe D. Tortell[1,6]

1. Department of Earth, Ocean and Atmospheric Sciences, University of British Columbia, Vancouver, BC, Canada. 2. Applied Ocean Physics and Engineering Department, Woods Hole, MA, USA. 3. Department of Aeronautics and Astronautics, Massachusetts Institute of Technology, Cambridge, MA, USA. 4. Department of Geography, University of Calgary, Calgary, AB, Canada. 5. Marine Chemistry and Geochemistry Department, Woods Hole Oceanographic Institution, Woods Hole, MA, USA. 6. Department of Botany, University of British Columbia, Vancouver, BC, Canada
† School of Earth and Ocean Sciences, University of Victoria, Victoria, BC, Canada.

Corresponding authors: Cara C. Manning (cmanning@alum.mit.edu), Anna Michel (amichel@whoi.edu), David Nicholson (dnicholson@whoi.edu)

Key Points:

- Methane concentrations in an Arctic estuary show strong seasonality; river inflow at the start of the freshet drives elevated concentrations
- Observations with a novel robotic kayak demonstrate that methane and carbon dioxide in the estuary are rapidly ventilated following ice melt
- River discharge is estimated to account for >95% of annual methane emissions from the estuary

Please cite the published manuscript:
Manning, C. C., Preston, V. L., Jones, S. F., Michel, A. P. M., Nicholson, D. P., Duke, P. J., et al.. (2020). River inflow dominates methane emissions in an Arctic coastal system. *Geophysical Research Letters*, 47, e2020GL087669. https://doi.org/10.1029/2020GL087669

EarthArXiv preprint of manuscript in press at *Geophysical Research Letters*
https://doi.org/10.1029/2020GL087669

Abstract

We present a year-round time series of dissolved methane (CH_4), along with targeted observations during ice melt of CH_4 and carbon dioxide (CO_2) in a river and estuary adjacent to Cambridge Bay, Nunavut, Canada. During the freshet, CH_4 concentrations in the river and ice-covered estuary were up to 240,000% saturation and 19,000% saturation, respectively, but quickly dropped by >100-fold following ice melt. Observations with a robotic kayak revealed that river-derived CH_4 and CO_2 were transported to the estuary and rapidly ventilated to the atmosphere once ice cover retreated. We estimate that river discharge accounts for >95% of annual CH_4 sea-to-air emissions from the estuary. These results demonstrate the importance of resolving seasonal dynamics in order to estimate greenhouse gas emissions from polar systems.

Plain Language Summary

The primary cause of recent global climate change is increasing concentrations of heat-trapping greenhouse gases in the atmosphere. Ongoing rapid Arctic climate change is affecting the annual cycle of sea ice formation and retreat, however most published studies of greenhouse gases in Arctic waters have been conducted during ice-free, summertime conditions. In order to characterize seasonal variability in greenhouse gas distributions, we collected year-round measurements of the greenhouse gas methane (CH_4) in a coastal Arctic system near Cambridge Bay, Nunavut, Canada. We found that during the ice melt season, river water contains methane concentrations up to 2000 times higher than the wintertime methane concentrations in the coastal ocean. We utilized a novel robotic kayak to conduct high-resolution mapping of greenhouse gas distributions during ice melt. From these data, we demonstrate that the river water containing elevated levels of methane and carbon dioxide (CO_2) flowed into the coastal ocean, and when ice cover melted, these greenhouse gases were rapidly emitted into the atmosphere. We estimate that in this system more than 95% of all annual methane emissions from the estuary are driven by river inflow.

1 Introduction

Methane (CH_4) emissions from Arctic waters and sediments may accelerate in the future as part of positive feedback from ongoing climate change (Biastoch et al., 2011; James et al., 2016; Shakhova et al., 2010). Landscapes that were once permanently frozen are now seasonally thawing, and the ice-free season is lengthening in freshwater and marine systems (Magnuson, 2000; Stroeve et al., 2012; Zona et al., 2016). Thawing can result in the mobilization of labile organic matter and emissions of greenhouse gases such as carbon dioxide (CO_2), methane (CH_4), and nitrous oxide (N_2O) (Karlsson et al., 2013; Kvenvolden et al., 1993; Lamarche-Gagnon et al., 2019; Voigt et al., 2017; Zona et al., 2016). Studies of terrestrial and freshwater Arctic systems have demonstrated strong temporal variability in greenhouse gas emissions in these environments (Denfeld et al., 2018; Karlsson et al., 2013; Lamarche-Gagnon et al., 2019; Phelps et al., 1998; Voigt et al., 2017; Zona et al., 2016), yet published measurements in Arctic marine and estuarine waters are strongly biased toward summertime, low-ice conditions (Fenwick et al., 2017; Shakhova et al., 2010), establishing a need for long-term studies that characterize the full range of seasonal variability.

Ice acts as a barrier to gas exchange, sustaining strong disequilibria in gas concentrations

between the atmosphere and ice-covered waters (Butterworth & Miller, 2016; Denfeld et al., 2018; Karlsson et al., 2013; Wand et al., 2006). Rapid re-equilibration of the mixed layer can occur following ice melt. Quantifying the impacts of sea ice loss on Arctic greenhouse gas emissions requires seasonally-resolved measurements; yet few measurements of dissolved CH_4 or other greenhouse gases are available in ice-covered or recently ice-liberated Arctic Ocean waters and connected estuaries. Here we present new observations that address this critical observational gap, demonstrating that the vast majority of annual CH_4 release in an Arctic estuary occurs during the ice melt period.

2 Observations, Results and Discussion

2.1 Field observations

To quantify the annual sea-air emissions of greenhouse gases in a coastal Arctic system, we collected measurements in a well-sheltered bay with two inlets (west arm and east arm, Figure 1a) adjacent to the town of Cambridge Bay (Iqaluktuuttiaq), Nunavut, Canada. Surface waters are seasonally ice covered, and the dominant freshwater source is Freshwater Creek, which discharges water into the east arm of Cambridge Bay from Greiner Lake and the associated watershed (mean annual discharge of 1.4×10^8 m^3 y^{-1} from 1970 to 2017). Terrestrial snowmelt in this region typically begins in late May (Tedesco et al., 2009), and, as a result, Freshwater Creek begins to flow before significant sea ice melt has occurred. This freshwater discharge causes the rapid melt of sea ice along the east arm, creating open water in June (Figure 1b), with the rest of the bay typically becoming ice-free 2–3 weeks later, in late June to early July. During 2017 and 2018, we collected a time-series of dissolved CH_4 and N_2O measurements in the estuary and river (Figures 1 and S1). Additionally, in 2018, we used a remotely operated robotic kayak, the ChemYak (Kimball et al., 2014; Nicholson et al., 2018), to characterize fine-scale spatiotemporal changes in dissolved CH_4 and CO_2 in the estuary during peak river inflow (Figures 2–3), and collected water samples from Greiner Lake. Methodological details for bottle samples and the ChemYak are provided in the Supporting Information. The datasets collected by the authors have been archived with PANGAEA (Manning et al., 2019).

During winter and spring (January–May) in 2017 and 2018, CH_4 concentrations throughout the estuary water column (station B1 in Fig. 1b) were closely distributed around the atmospheric equilibrium of 4 nM (range 3–10 nM). In early June, river discharge from the spring thaw began to enter the estuary, and elevated CH_4 concentrations up to 860 nM (19,000% saturation) were measured in near-surface waters of Cambridge Bay (2 m below the surface of the ice). A water mass analysis using salinity and water isotope data from station B1 confirmed that the elevated CH_4 concentrations were associated with river runoff rather than ice melt (Figure S2 and Text S1). Ice-free summer surface waters sampled in July 2017 and 2018 had much lower CH_4 concentrations, ranging from 4–65 nM.

In contrast to CH_4, N_2O concentrations throughout 2017-2018 at station B1 and Freshwater Creek displayed limited seasonal variability and were close to equilibrium (Figure S1 and Text S2).

From 28 June to 2 July 2018, we used the ChemYak for high-resolution spatial mapping and vertical profiling of CH_4, CO_2, salinity, and temperature distributions in a ~1 km^2 open water

area between the river mouth and the ice edge during the dynamic melt period (Figures 2, 3 and S3–S6). These ChemYak measurements confirmed elevated greenhouse gas concentrations in river-derived estuary water. The river-derived water occurred throughout the study area as a shallow, fresh surface mixed layer (<2 m depth), separated from deeper waters by a sharp pycnocline (Figure 2 f-g). During the ChemYak measurement period, CH_4 concentrations in the surface water decreased each day and as the water flowed from the river toward the coastal ocean, suggesting a rapid ventilation within the estuary. For example, the CH_4 concentration in Freshwater Creek decreased from 560±10 nM on 27 June to 290±20 nM by 3 July, whereas CH_4 at station B1 was 130±10 nM on 3 July (Figure 4b). In the ChemYak sampling area (between Freshwater Creek and station B1), on 28 June, CH_4 and CO_2 concentrations in the upper 1 m of the water column were up to 470 nM and 1470 µatm, respectively (mean 410±20 nM and 1340±40 µatm). Concentrations in the upper 1 m decreased over the campaign to 150±70 nM CH_4 and 600±150 µatm CO_2 by 2 July (Figures 3 and S6).

EarthArXiv preprint of manuscript in press at *Geophysical Research Letters*
https://doi.org/10.1029/2020GL087669

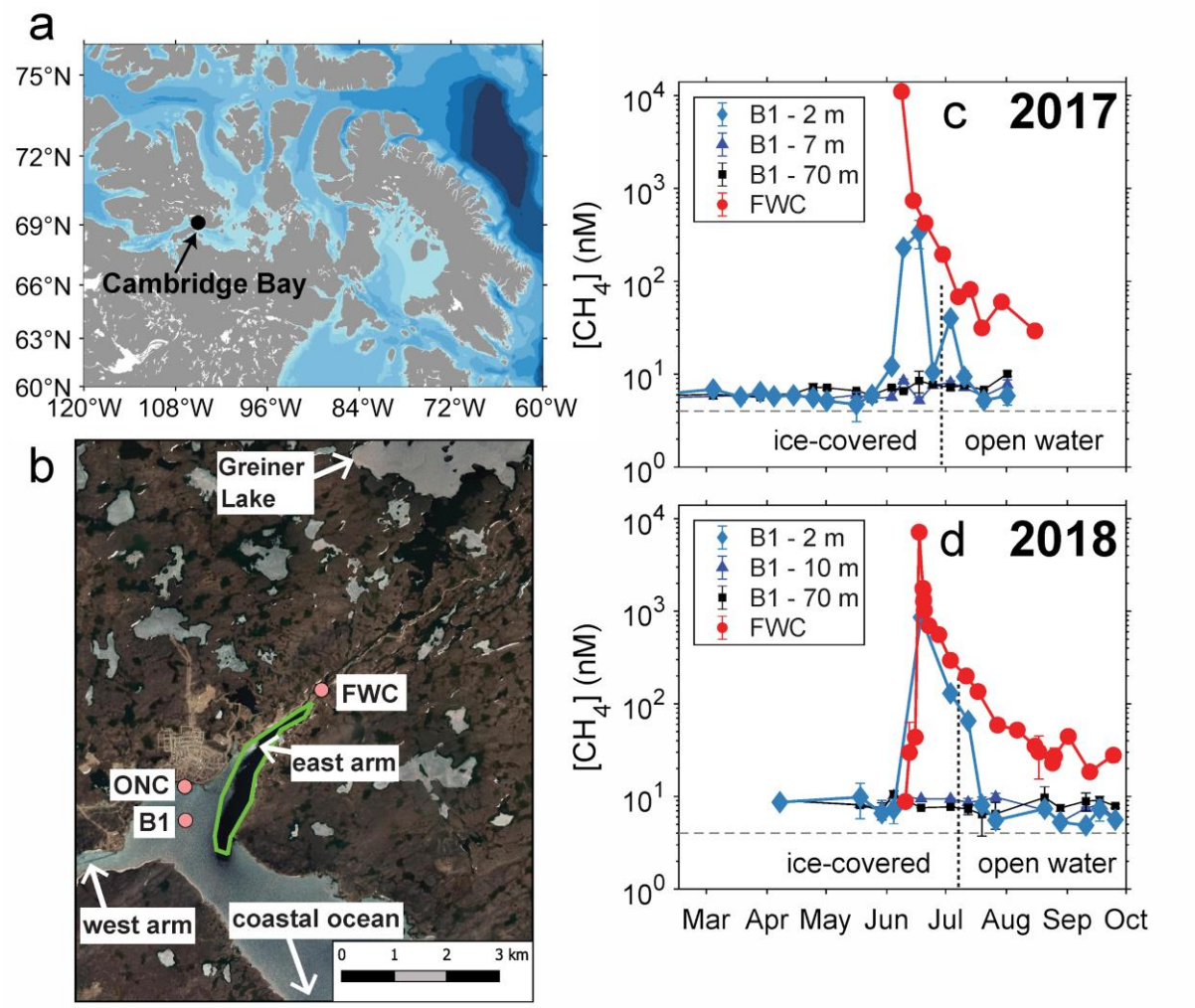

Figure 1. Map of study site and time-series data. **a** Map of eastern Canadian Arctic showing the location of Cambridge Bay. **b** Satellite image of study area on 21 June 2017 (obtained by Google, DigitalGlobe). Pink circles indicate the locations of the main sampling stations FWC (Freshwater Creek) and B1, as well as ONC (Ocean Networks Canada observatory with ice profiler). The approximate region where the ChemYak was deployed is shown with a green outline. Time-series of CH_4 concentrations in Cambridge Bay estuary and Freshwater Creek in **c** 2017 and **d** 2018. Surface samples in Cambridge Bay were collected at 2 m depth below the ice surface, or 0.75 m below the open water surface. The dashed horizontal line represents atmospheric equilibrium and the dashed vertical line indicates when sampling station B1 became ice-free. Error bars reflect the standard deviation of duplicate measurements.

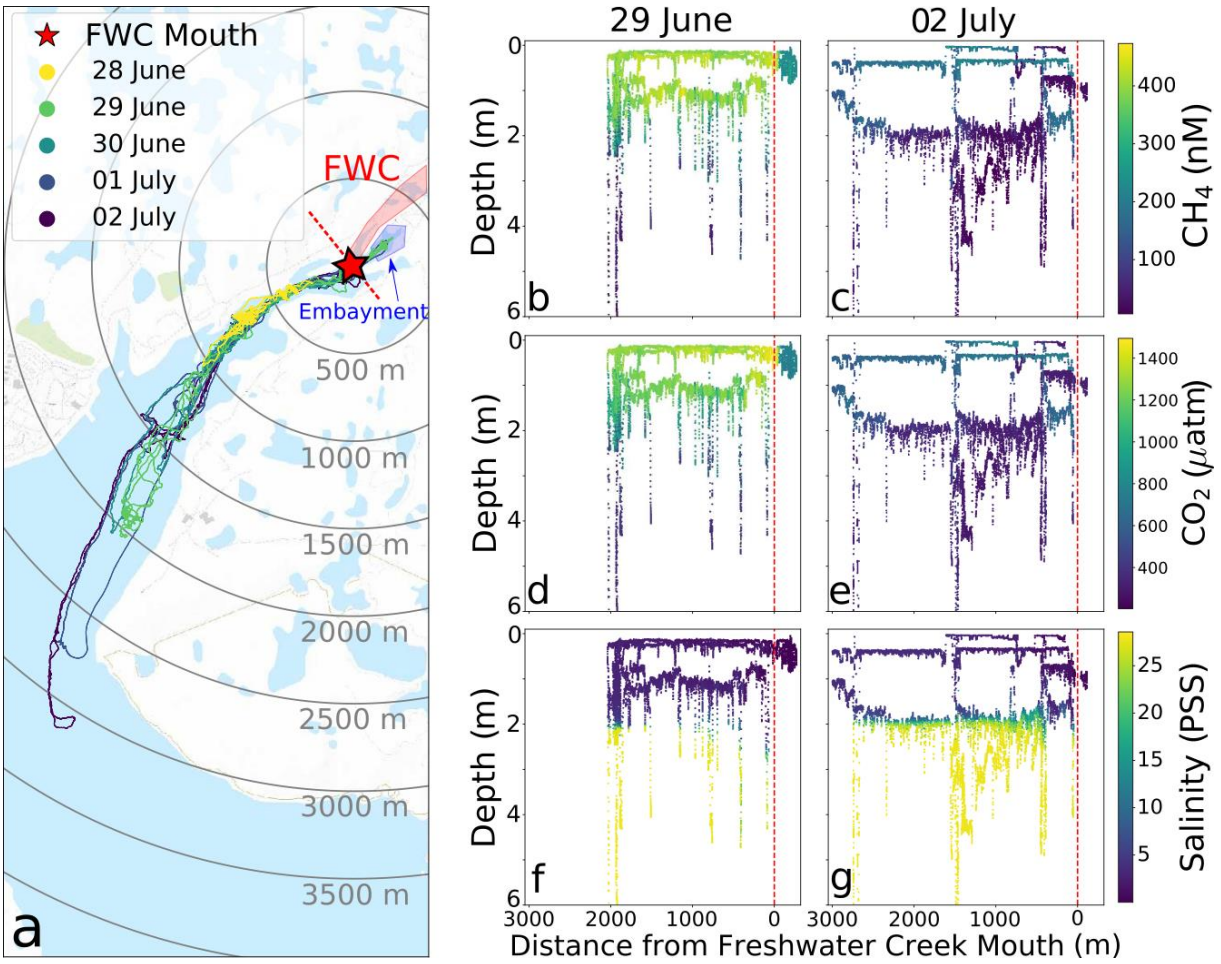

Figure 2. Spatial observations made by the ChemYak vehicle. **a** The study site with ChemYak trajectories from each day overlaid. The mouth of Freshwater Creek (69.1257 ºN, 105.0042 ºW) is marked with a star, and concentric rings at increments of 500 m centered at the mouth are provided for scale. Northeast of the red dashed line lies Freshwater Creek (red arrow and box) and a small embayment (blue label and box) which receives input from a much smaller river. **b-g** Observations made by the ChemYak for two representative days, 29 June and 2 July, are plotted by depth versus distance from the Freshwater Creek mouth. Negative distances (to the right of the axis) represent points northeast of the mouth (a small embayment) and positive distance (to the left of the axis) represent points southwest of the mouth (downstream). As indicated by the salinity plots (**f-g**), the mixed layer depth is <2 m throughout the study area, and the fresh surface layer was generally higher in both CH_4 and CO_2 concentration than layers deeper than 2 m. The gas concentrations decreased over the multi-day measurement campaign. Equivalent plots and temperature data for the other measurement days are shown in Figure S5.

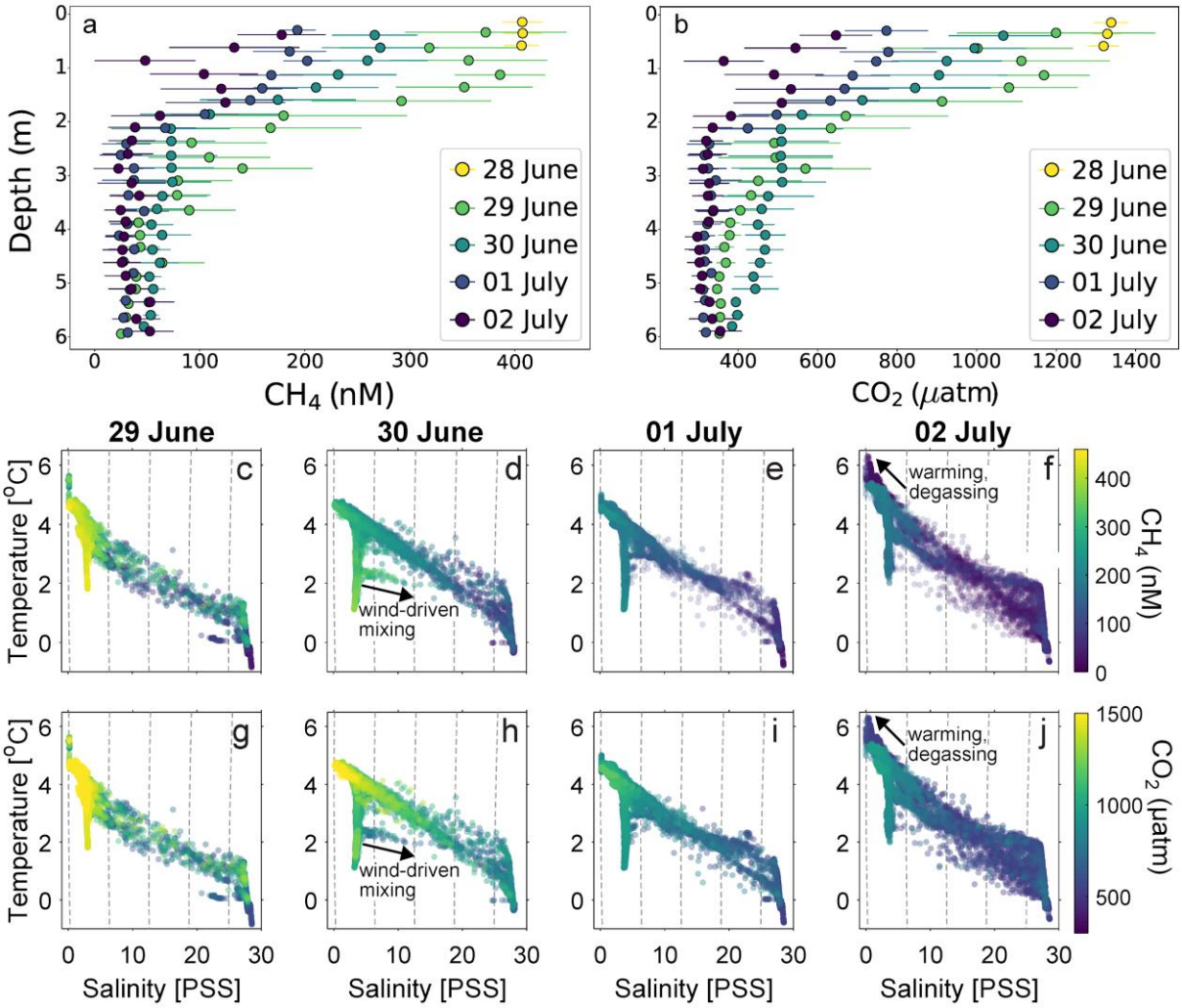

Figure 3. Spatial and temporal trends observed by the ChemYak. **a-b** Each day of the measurement campaign is marked with a unique color, and samples collected are binned into 0.25 m increments from the surface to 6 m. Both CH_4 (**a**) and CO_2 (**b**) exhibit decreasing trends for each subsequent day, and there is strong stratification between the surface layer and water below 2 m. Error bars represent the standard deviation of measurements for each depth bin. **c-j** Temperature-salinity plots showing changes in CH_4 (**c-f**) and CO_2 (**g-j**) concentrations and water mass distributions over the time-series.

In the estuary, at depths below the mixed layer (>2 m depth), CH_4 and CO_2 concentrations decreased from 29 June to 2 July. Elevated wind speeds (up to 10 m s^{-1}) appear to have enhanced mixing across the sharp pycnocline on 30 June (Figures 3d, 3h, S5, and S6). On 30 June, the depth of the pycnocline shoaled and CH_4 and CO_2 concentrations below the mixed layer increased near the ice edge and the river mouth. Over the following days, lower wind speeds (3.7±1.1 m s^{-1}), coupled with decreasing river inflow concentrations and restratification of the water column, led to decreased gas concentrations throughout the water column by 2 July. Changes in the observed temperature-salinity properties of the water suggest that mixing reduced the vertical salinity gradient over the measurement period. The mixed layer near the river mouth showed significant warming between 28 June and 2 July (Figures 3c-j, S5, and S6).

To evaluate the importance of atmospheric ventilation to the CH_4 budget in the estuary, we performed sea-air flux calculations (Wanninkhof, 2014) using observed wind speeds. In the absence of lateral transport and river discharge, CH_4 concentrations in the estuary over our sampling period would be expected to decrease to ~70 nM. In actuality, we observed a mean surface CH_4 concentration of ~150 nM at the end of the sampling period, suggesting that the continued inflow of high-CH_4 river water into the ChemYak sampling region contributed to maintaining elevated CH_4 concentrations following ice melt (Figure 4a). Based on the observed river discharge of ~40 m^3 s^{-1}, we estimate that the residence time of water in the ChemYak measurement region was ~0.6 d.

In addition to measuring the estuary downstream of the Freshwater Creek mouth, the ChemYak was also used to collect observations in a small embayment at the outlet of a much smaller river on 29 June, 1 July, and 2 July (Figures 2, 3, S4, and S5). We present the results from this embayment to highlight the complexities of quantifying greenhouse gas fluxes from estuarine systems. This embayment generally exhibited higher temperatures and lower CH_4 and CO_2 concentrations relative to adjacent waters. For example, on 29 June, the mean CH_4 concentration in the upper 2 m was 242±41 nM in the embayment (upstream of the Freshwater Creek mouth), in contrast to 417±31 nM within 100 m downstream of the Freshwater Creek mouth (Figure 2b). For CO_2, the mean concentration was 790±140 μatm in the embayment and 1400±110 μatm downstream of the Freshwater Creek mouth. In late June to early July 2018, we collected bottle samples at the head of the embayment in this smaller river and found that CH_4 concentrations in Freshwater Creek were two times higher than in the smaller river. The CH_4 and CO_2 levels in the embayment may therefore reflect lower inflowing CH_4 and CO_2 from the smaller river, and/or a longer residence time for river-derived surface water to exchange with the atmosphere in the embayment. The observed differences between the smaller river and embayment compared to Freshwater Creek and the rest of the estuary demonstrate the need to conduct studies in a diverse range of Arctic coastal systems to better understand the complex hydrological controls on the magnitude and location of greenhouse gas emissions.

Overall, we conclude that the declining CH_4 and CO_2 concentrations throughout the water column between 28 June and 2 July, and along the spatial gradient from Freshwater Creek to station B1, primarily reflect a combination of decreasing gas concentrations in the river water (Figure 1c), loss due to gas exchange within the ice-liberated area, and oceanward lateral advective export. Below, we present a physical model for the estuarine mixed layer CH_4 budget, and discuss potential impacts of microbial processes on the CH_4 budget.

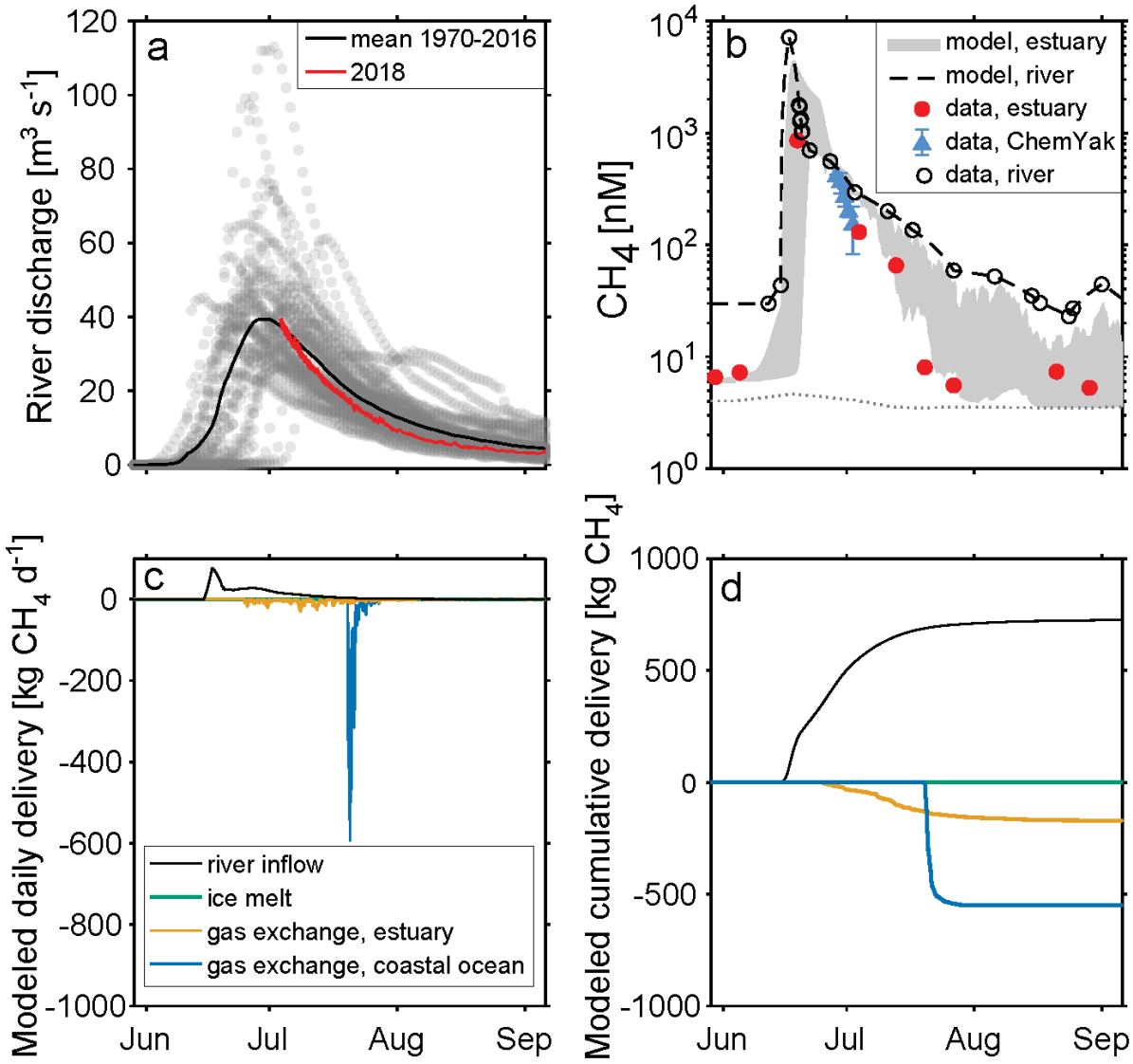

Figure 4. Observations and model-derived output of CH_4 delivery to the estuary mixed layer. **a** Historical river discharge data from Freshwater Creek. **b** Modeled and measured CH_4 concentration in the river (Freshwater Creek) and the Cambridge Bay estuary mixed layer (Model Regions 1 and 2), based on data and the model. The range of modeled values across the estuary is shown with grey shading and the range of values measured with the ChemYak is shown with blue symbols (error bars represent the standard deviation of daily measurements). The red symbols represent bottle measurements at station B1, and the black outlined symbols represent measurements at Freshwater Creek. The grey dotted line shows the equilibrium concentration in the estuary. **c-d** Modeled daily (**c**) and cumulative (**d**) CH_4 delivery to the estuary, from river inflow, ice melt, and gas exchange (positive delivery represents an input to the mixed layer). The CH_4 delivery caused by ice melt is negligible relative to the other terms.

2.2 Mixed layer model

To quantify the fate of river-derived CH_4 over the entire river inflow season, we developed a mixed layer model for the Cambridge Bay estuary (Figures 4 and S7). The model was constrained with measured CH_4 concentrations in Freshwater Creek (bottle samples), river discharge and wind speed measurements, and ice thickness records from the Ocean Networks Canada (ONC) cabled observatory. The model is described in detail in the Supporting Information (Figure S8 and Text S3) and the model code, including all input data, is available on GitHub (http://doi.org/10.5281/zenodo.3749430). The results of this analysis suggest that the annual CH_4 cycle in the estuary is driven by river inflow, with sea ice melt contributing a comparatively negligible amount of CH_4 to the mixed layer (Figure 4d). This conclusion is consistent with a water mass property (salinity/water isotope) analysis showing an insignificant impact of sea ice melt on the CH_4 budget (Figure S2 and Text S1).

Using the model, we estimate that ~730 kg CH_4 was released from Freshwater Creek into the estuary in 2018 (volume-weighted mean concentration in river water of 360 nM), with 24% (177 kg) ventilated to the atmosphere from the estuary following ice cover retreat (Figure 4d). The remaining 76% of the river-derived CH_4 was laterally transported across the estuary beneath sea ice to the coastal ocean, where it was likely ventilated to the atmosphere following ice melt in mid-late July. Indeed, a model run with a larger spatial footprint (including 60 km^2 of coastal ocean surrounding the 5 km^2 Cambridge Bay estuary) yielded a cumulative annual sea-air emission of 548 kg CH_4 from the coastal ocean derived from river discharge, which occurs rapidly following ice melt (Figure 4d). To estimate the CH_4 emissions from the estuary in the absence of river inflow, we prescribe a fixed CH_4 concentration of 6 nM (~150% saturation), the typical surface concentration before and after the river inflow period. Under this scenario, with no river discharge, we derived annual estuarine CH_4 emissions of 7.4 kg, 24 times lower than the emissions derived from the full model including riverine CH_4 inputs. Given that our model predicts that 76% of the riverine CH_4 is ventilated beyond the estuary in the adjacent coastal ocean, small river systems such as Freshwater Creek may be of primary importance to annual CH_4 budgets through much of the coastal Arctic Ocean. Accurate calculation of such short-lived, high magnitude CH_4 emissions following ice melt, requires a more extensive under-ice sampling program, including melt-season measurements in multiple river-influenced Arctic estuaries and coastal systems.

The extent of microbial CH_4 oxidation in river-derived water discharged from Freshwater Creek is currently unknown. The early-season river discharge containing >1000 nM CH_4 may remain under the ice for ~1 month before being exposed to the atmosphere, during which time microbial oxidation could potentially decrease CH_4 levels. Recent incubation studies measuring CH_4 oxidation rates and rate constants in Arctic waters and ice-covered lakes have reported a wide range of values (Bastviken et al., 2002; Bussmann et al., 2017; Gentz et al., 2014; Mau et al., 2013; Ricão Canelhas et al., 2016; Uhlig & Loose, 2017). For example, in an Arctic fjord, Mau et al. (2013) reported first-order CH_4 oxidation rate constants ranging over three orders of magnitude, from ~0.0001 to 0.1 d^{-1}. To determine the maximum possible impact of CH_4 oxidation on the CH_4 budget, we tested a model run incorporating CH_4 oxidation with a rate constant of 0.1 d^{-1} (Text S3 and Figure S9). With this high rate of CH_4 oxidation, the modeled annual CH_4 emissions within the estuary decreased only slightly (from 177 to 164 kg), but CH_4 emissions from the adjacent coastal ocean decreased significantly (from 540 to 130 kg). An

oxidation rate of 0.01 d^{-1} yielded emissions of 175 kg and 480 kg for the estuary and coastal ocean respectively (Figure S9). Overall, these results suggest that microbial oxidation could potentially contribute to a significant reduction in the fraction of laterally exported CH_4 that ultimately is emitted to the atmosphere, but likely has a small impact on CH_4 emissions within the Cambridge Bay estuary. In the future, we hope to measure CH_4 concentration in the coastal ocean adjacent to Cambridge Bay estuary, and CH_4 oxidation rates in Cambridge Bay and adjacent waters, and use these data to improve the model.

3 Conclusions and future work

Our results, derived from a year-round times series of CH_4 measurements and dense spatio-temporal observations from a remotely-operated robotic kayak, show that CH_4 discharge via Freshwater Creek drives intense CH_4 emissions immediately following ice melt in the Cambridge Bay estuary and surrounding waters. River discharge also acts as a significant seasonal source of CO_2 to the estuary. This study demonstrates the importance of fully resolving seasonal processes in inter-connected marine and freshwater Arctic environments to accurately quantify greenhouse gas emissions. We have also demonstrated the advantages of using new sensing technologies to study heterogeneous and dynamic systems. Similar seasonal variability in CH_4 emissions likely occurs in some other river-influenced, seasonally ice-covered Arctic estuaries, which receive ~10% of global river discharge (Dai & Trenberth, 2002). More field studies in a wide range of Arctic river and coastal systems are needed to determine the impact of ongoing and projected future increases in Arctic river discharge (Macdonald et al., 2015) on greenhouse gas emissions. For example, more extensive measurements of CH_4 concentration and isotopic composition across the land-ocean continuum would assist in determining CH_4 and CO_2 sources and sinks. Radiocarbon measurements would demonstrate whether ancient CH_4 sources such as thawing permafrost are significant (Sparrow et al., 2018). Such studies will provide critical information to characterize current and future Arctic greenhouse gas cycling, improving quantitative estimates of changes in CH_4 and CO_2 emissions.

The low and stable CH_4 concentrations observed below the mixed layer in the Cambridge Bay estuary indicate that sedimentary CH_4 sources within this estuary are negligible relative to river-derived inputs, in contrast to published studies in some other Arctic coastal and shelf systems where significant sedimentary sources are observed (Gentz et al., 2014; Shakhova et al., 2010). Therefore, more research is needed in a wide range of Arctic coastal waters to more accurately characterize the relative importance of terrestrial sources versus subseafloor deposits.

Freshwater input to the Canadian Arctic Archipelago is dominated by small river systems such Freshwater Creek with a collective discharge on the same order as large rivers such as the Mackenzie (Alkire et al. 2017), yet these small rivers are rarely sampled due to challenging conditions. The CH_4 concentrations we measured in Freshwater Creek (ranging from 10–11000 nM, volume-weighted mean 360 nM) are similar to other river systems in the Arctic and worldwide. For example, mean CH_4 concentrations observed in the Yukon River, Lena Delta, and Leverett Glacier runoff range from 70–750 nM (Bussmann, 2013; Lamarche-Gagnon et al., 2019; Striegl et al., 2012). Furthermore, a data compilation of over 900 rivers and streams worldwide reported a mean CH_4 concentration of 1400 ± 5200 nM and median of 250 nM (Stanley et al., 2016). The peak CH_4 concentrations observed in Cambridge Bay estuary (up to

900 nM during the freshet, prior to ice melt) are similar to maximum values measured in other Arctic coastal waters (Bussmann et al., 2017; Shakhova et al., 2010).

The results of this study motivate future coastal Arctic field campaigns at other sites with measurement technologies capable of high spatial and temporal resolution mapping immediately before and during ice melt. Such studies will provide critical information to characterize current and future Arctic greenhouse gas emission, improving quantitative estimates of changes in CH_4 and CO_2 emissions across the rapidly changing Arctic environment.

Acknowledgments, Samples, and Data

All data generated by the authors that were used in this article are available on PANGAEA (https://doi.org/10.1594/PANGAEA.907159) and model code for estimating CH_4 transport is available on GitHub (https://doi.org/10.5281/zenodo.3785893). We acknowledge the use of imagery from the NASA Worldview application (https://worldview.earthdata.nasa.gov), part of the NASA Earth Observing System Data and Information System (EOSDIS), and data from Ocean Networks Canada, and Environment Canada. We thank everyone involved in the fieldwork including C. Amegainik, Y. Bernard, A. Cranch, F. Emingak, S. Marriott, and A. Pedersen. Laboratory analysis and experiments were performed by A. Cranch, R. McCulloch, A. Morrison, and Z. Zheng. We thank J. Brinckerhoff, the Arctic Research Foundation, and the staff of the Canadian High Arctic Research Station for support with field logistics. Funding for the work was provided by MEOPAR NCE funding to B. Else, a WHOI Interdisciplinary Award to A. Michel., D. Nicholson. and S. Wankel, and Canadian NSERC grants to P. Tortell. and B. Else. Authors received fellowships, scholarships and travel grants including an NSERC postdoctoral fellowship to C. Manning, an NDSEG fellowship to V. Preston, NSERC PGS-D and Izaak Walton Killam Pre-Doctoral scholarships to S. Jones, and Northern Scientific Training Program funds (Polar Knowledge Canada, administered by the Arctic Institute of North America, University of Calgary) to S. Jones and P. Duke. We also thank Polar Knowledge Canada (POLAR) and Nunavut Arctic College for laboratory space and field logistics support.

References

Alkire, M.B., Jacobson, A.D., Lehn, G.O., Macdonald, R.W. & Rossi, M.W. (2017). On the geochemical heterogeneity of rivers draining into the straits and channels of the Canadian Arctic Archipelago. *Journal of Geophysical Research: Biogeosciences*, *122*(10), 2527-2547. https://doi.org/10.1002/2016JG003723

Anderson, L.G., Turner, D.R., Wedborg, M. & Dyrssen, D. (1999). Determination of total alkalinity and total dissolved inorganic carbon. *In:* Methods of Seawater Analysis, Grasshoff, K., Kremling, K. & Ehrhardt, M., eds. pp. 127-148.

Bastviken, D., Ejlertsson, J., & Tranvik, L. (2002). Measurement of methane oxidation in lakes: a comparison of methods. *Environmental Science & Technology*, *36*(15), 3354-3361. https://doi.org/10.1021/es010311p

Biastoch, A., Treude, T., Rüpke, L. H., Riebesell, U., Roth, C., Burwicz, E. B., et al. (2011). Rising Arctic Ocean

temperatures cause gas hydrate destabilization and ocean acidification. *Geophysical Research Letters*, *38*(8). https://doi.org/10.1029/2011GL047222

Bliss, L. C. (1981). North American and Scandinavian tundras and polar deserts. In L. C. Bliss, O. W. Heal, & J. J. Moore (Eds.), *Tundra ecosystems: a comparative analysis* (pp. 8–24). Cambridge, UK: Cambridge University Press.

Bussmann, I. (2013). Distribution of methane in the Lena Delta and Buor-Khaya Bay, Russia. *Biogeosciences*, *10*(7), 4641–4652. https://doi.org/10.5194/bg-10-4641-2013

Bussmann, I., Hackbusch, S., Schaal, P., & Wichels, A. (2017). Methane distribution and oxidation around the Lena Delta in summer 2013. *Biogeosciences*, *14*(21), 4985–5002. https://doi.org/10.5194/bg-14-4985-2017

Butterworth, B. J., & Miller, S. D. (2016). Air-sea exchange of carbon dioxide in the Southern Ocean and Antarctic marginal ice zone. *Geophysical Research Letters*, *43*(13), 7223–7230. https://doi.org/10.1002/2016GL069581

Cai, W.-J., Hu, X., Huang, W.-J., Jiang, L.-Q., Wang, Y., Peng, T.-H., & Zhang, X. (2010). Alkalinity distribution in the western North Atlantic Ocean margins. *Journal of Geophysical Research: Oceans*, *115*(C8). https://doi.org/10.1029/2009JC005482

Capelle, D. W., Dacey, J. W., & Tortell, P. D. (2015). An automated, high through-put method for accurate and precise measurements of dissolved nitrous-oxide and methane concentrations in natural waters: Automated PT-GCMS for N_2O and CH_4. *Limnology and Oceanography: Methods*, *13*(7), 345–355. https://doi.org/10.1002/lom3.10029

Dai, A., & Trenberth, K. E. (2002). Estimates of Freshwater Discharge from Continents: Latitudinal and Seasonal Variations. *Journal of Hydrometeorology*, *3*(6), 660–687. https://doi.org/10.1175/1525-7541(2002)003<0660:EOFDFC>2.0.CO;2

Denfeld, B. A., Baulch, H. M., Giorgio, P. A. del, Hampton, S. E., & Karlsson, J. (2018). A synthesis of carbon dioxide and methane dynamics during the ice-covered period of northern lakes. *Limnology and Oceanography Letters*, *3*(3), 117–131. https://doi.org/10.1002/lol2.10079

Dickson, A. G. (1990). Thermodynamics of the dissociation of boric acid in synthetic seawater from 273.15 to 318.15 K. *Deep Sea Research Part A. Oceanographic Research Papers*, *37*(5), 755–766. https://doi.org/10.1016/0198-0149(90)90004-F

Environment and Climate Change Canada Historical Hydrometric Data website, River discharge data for station 10TF001, Freshwater Creek near Cambridge Bay https://wateroffice.ec.gc.ca/mainmenu/historical_data_index_e.html. Water Survey of Canada, Environment and Climate Change Canada. Downloaded on January 10, 2019.

Environment and Climate Change Canada Historical Database (2019) Hourly weather data for Cambridge Bay, Nunavut from Jan 1, 2018 to Jan 1, 2019. Station Climate ID: 2400602, WMO ID: 71288 TC ID: XCM http://climate.weather.gc.ca . Downloaded on February 25, 2019.

Fenwick, L., Capelle, D., Damm, E., Zimmermann, S., Williams, W. J., Vagle, S., & Tortell, P. D. (2017). Methane and nitrous oxide distributions across the North American Arctic Ocean during summer, 2015. *Journal of Geophysical Research: Oceans*, 1–23. https://doi.org/10.1002/2016JC012493

Gentz, T., Damm, E., Schneider von Deimling, J., Mau, S., McGinnis, D. F., & Schlüter, M. (2014). A water column study of methane around gas flares located at the West Spitsbergen continental margin. *Continental Shelf Research*, *72*, 107–118. https://doi.org/10.1016/j.csr.2013.07.013

James, R. H., Bousquet, P., Bussmann, I., Haeckel, M., Kipfer, R., Leifer, I., et al. (2016). Effects of climate change on methane emissions from seafloor sediments in the Arctic Ocean: A review. *Limnology and Oceanography*, *61*(S1), S283–S299. https://doi.org/10.1002/lno.10307

Karlsson, J., Giesler, R., Persson, J., & Lundin, E. (2013). High emission of carbon dioxide and methane during ice thaw in high latitude lakes. *Geophysical Research Letters*, *40*(6), 1123–1127. https://doi.org/10.1002/grl.50152

Kimball, P., Bailey, J., Das, S., Geyer, R., Harrison, T., Kunz, C., et al. (2014). The WHOI Jetyak: An autonomous surface vehicle for oceanographic research in shallow or dangerous waters. *2014 IEEE/OES Autonomous Underwater Vehicles (AUV)*, 1–7. https://doi.org/10.1109/AUV.2014.7054430

Kvenvolden, K. A., Lilley, M. D., Lorenson, T. D., Barnes, P. W., & McLaughlin, E. (1993). The Beaufort Sea continental shelf as a seasonal source of atmospheric methane. *Geophysical Research Letters*, *20*(22), 2459–2462. https://doi.org/10.1029/93GL02727

Lamarche-Gagnon, G., Wadham, J. L., Sherwood Lollar, B., Arndt, S., Fietzek, P., Beaton, A. D., et al. (2019). Greenland melt drives continuous export of methane from the ice-sheet bed. *Nature*, *565*(7737), 73–77. https://doi.org/10.1038/s41586-018-0800-0

Lee, K., Kim, T.-W., Byrne, R. H., Millero, F. J., Feely, R. A., & Liu, Y.-M. (2010). The universal ratio of boron to chlorinity for the North Pacific and North Atlantic oceans. *Geochimica et Cosmochimica Acta*, *74*(6), 1801–1811. https://doi.org/10.1016/j.gca.2009.12.027

Macdonald, R. W., Kuzyk, Z. A., & Johannessen, S. C. (2015). It is not just about the ice: a geochemical perspective on the changing Arctic Ocean. *Journal of Environmental Studies and Sciences*, *5*(3), 288–301. https://doi.org/10.1007/s13412-015-0302-4

Macdonald, R. W., Paton, D. W., Carmack, E. C., & Omstedt, A. (1995). The freshwater budget and under-ice spreading of Mackenzie River water in the Canadian Beaufort Sea based on salinity and 18O/16O measurements in water and ice. *Journal of Geophysical Research: Oceans*, *100*(C1), 895–919. https://doi.org/10.1029/94JC02700

Magnuson, J. J. (2000). Historical Trends in Lake and River Ice Cover in the Northern Hemisphere. *Science*, *289*(5485), 1743–1746. https://doi.org/10.1126/science.289.5485.1743

Manning, C. C.; Preston, V. L., Jones, S. F., Michel, A. P. M., Nicholson, D. P., Duke, P. J., Ahmed, M. M. M., Manganini, K., Else, B. G. T., & Tortell, P. T. (2019): Dissolved methane, nitrous oxide, carbon dioxide, water isotope, salinity and temperature data from Cambridge Bay, Nunavut, Canada (2017-2018). *PANGAEA*, https://doi.org/10.1594/PANGAEA.907159

Manning, C. C., & Preston, V. L. (2020). caramanning/cambridge-bay-model: Cambridge Bay model with optional methane oxidation term (Version v1.3). *Zenodo*. https://doi.org/10.5281/zenodo.3785893

Mau, S., Blees, J., Helmke, E., Niemann, H., & Damm, E. (2013). Vertical distribution of methane oxidation and methanotrophic response to elevated methane concentrations in stratified waters of the Arctic fjord Storfjorden (Svalbard, Norway). *Biogeosciences*, *10*, 6267-6278. https://doi.org/10.5194/bg-10-6267-2013

Millero, F. J. (2010). Carbonate constants for estuarine waters. *Marine and Freshwater Research*, *61*(2), 139–142. https://doi.org/10.1071/MF09254

Naqvi, S. W. A., Bange, H. W., Farías, L., Monteiro, P. M. S., Scranton, M. I., & Zhang, J. (2010). Marine hypoxia/anoxia as a source of CH_4 and N_2O. *Biogeosciences*, *7*(7), 2159–2190. https://doi.org/10.5194/bg-7-2159-2010

Nicholson, D. P., Michel, A. P. M., Wankel, S. D., Manganini, K., Sugrue, R. A., Sandwith, Z. O., & Monk, S. A. (2018). Rapid Mapping of Dissolved Methane and Carbon Dioxide in Coastal Ecosystems Using the

ChemYak Autonomous Surface Vehicle. *Environmental Science & Technology*. https://doi.org/10.1021/acs.est.8b04190

Ocean Networks Canada Data Archive (2019) Corrected ice draft data from Cambridge Bay, Nunavut, from Jan 1, 2018 to Jan 1, 2019. http://www.oceannetworks.ca, Ocean Networks Canada, University of Victoria, Canada. Downloaded on May 25, 2019.

Phelps, A. R., Peterson, K. M., & Jeffries, M. O. (1998). Methane efflux from high-latitude lakes during spring ice melt. *Journal of Geophysical Research: Atmospheres*, *103*(D22), 29029–29036. https://doi.org/10.1029/98JD00044

Pierrot, D., Lewis, E., & Wallace, D. W. R. (2006). *MS Excel Program Developed for CO2 System Calculations* (Technical Report). Oak Ridge, Tenn: Carbon Dioxide Inf. Anal. Cent., Oak Ridge Natl. Lab., US DOE.

Ricão Canelhas, M., Denfeld, B. A., Weyhenmeyer, G. A., Bastviken, D., & Bertilsson, S. (2016). Methane oxidation at the water-ice interface of an ice-covered lake. Limnology and Oceanography, 61(S1), S78-S90.

Seitzinger, S. P., & Kroeze, C. (1998). Global Distribution of Nitrous Oxide Production and N Inputs in Freshwater and Coastal Marine Ecosystems, *12*(1), 93–113.

Seitzinger S.P., Kroeze C., & Styles R.V. (2000). Global distribution of N2O emissions from aquatic systems: natural emissions and anthropogenic effects. *Chemosphere: Global Change Science*, *2*, 267–279. https://doi.org/10.1016/S1465-9972(00)00015-5

Shakhova, N., Semiletov, I., Salyuk, A., Yusupov, V., Kosmach, D., & Gustafsson, Ö. (2010). Extensive Methane Venting to the Atmosphere from Sediments of the East Siberian Arctic Shelf. *Science*, *327*(5970), 1246–1250. https://doi.org/10.1126/science.1182221

Sparrow, K. J., Kessler, J. D., Southon, J. R., Garcia-Tigreros, F., Schreiner, K. M., Ruppel, C. D., et al. (2018). Limited contribution of ancient methane to surface waters of the U.S. Beaufort Sea shelf. *Science Advances*, *4*(1), eaao4842. https://doi.org/10.1126/sciadv.aao4842

Stanley, E. H., Casson, N. J., Christel, S. T., Crawford, J. T., Loken, L. C., & Oliver, S. K. (2016). The ecology of methane in streams and rivers: Patterns, controls, and global significance. *Ecological Monographs*, *86*(2), 146–171. https://doi.org/10.1890/15-1027.1

Striegl, R. G., Dornblaser, M. M., McDonald, C. P., Rover, J. R., & Stets, E. G. (2012). Carbon dioxide and methane emissions from the Yukon River system. *Global Biogeochemical Cycles*, *26*(4).

https://doi.org/10.1029/2012GB004306

Stroeve, J. C., Serreze, M. C., Holland, M. M., Kay, J. E., Malanik, J., & Barrett, A. P. (2012). The Arctic's rapidly shrinking sea ice cover: a research synthesis. *Climatic Change*, *110*(3–4), 1005–1027. https://doi.org/10.1007/s10584-011-0101-1

Tedesco, M., Brodzik, M., Armstrong, R., Savoie, M. & Ramage, J. (2009). Pan arctic terrestrial snowmelt trends (1979–2008) from spaceborne passive microwave data and correlation with the Arctic Oscillation. *Geophysical Research Letters*, *36*(21). https://doi.org/10.1029/2009GL039672

Uhlig, C., & Loose, B. (2017). Using stable isotopes and gas concentrations for independent constraints on microbial methane oxidation at Arctic Ocean temperatures. *Limnology and Oceanography: Methods*, *15*(8), 737–751. https://doi.org/10.1002/lom3.10199

Voigt, C., Marushchak, M. E., Lamprecht, R. E., Jackowicz-Korczyński, M., Lindgren, A., Mastepanov, M., et al. (2017). Increased nitrous oxide emissions from Arctic peatlands after permafrost thaw. *Proceedings of the National Academy of Sciences*, *114*(24), 6238–6243. https://doi.org/10.1073/pnas.1702902114

Wand, U., Samarkin, V. A., Nitzsche, H.-M., & Hubberten, H.-W. (2006). Biogeochemistry of methane in the permanently ice-covered Lake Untersee, central Dronning Maud Land, East Antarctica. *Limnology and Oceanography*, *51*(2), 1180–1194. https://doi.org/10.4319/lo.2006.51.2.1180

Wanninkhof, R. (2014). Relationship between wind speed and gas exchange over the ocean revisited. *Limnology and Oceanography: Methods*, *12*(6), 351–362. https://doi.org/10.4319/lom.2014.12.351

Weiss, R. F., & Price, B. A. (1980). Nitrous oxide solubility in water and seawater. *Marine Chemistry*, *8*(4), 347–359. https://doi.org/10.1016/0304-4203(80)90024-9

Wiesenburg, D. A., & Guinasso, N. L. (1979). Equilibrium solubilities of methane, carbon monoxide, and hydrogen in water and sea water. *Journal of Chemical & Engineering Data*, *24*(4), 356–360. https://doi.org/10.1021/je60083a006

Wilson, S. T., Bange, H. W., Arévalo-Martínez, D. L., Barnes, J., Borges, A. V., Brown, I., et al. (2018). An intercomparison of oceanic methane and nitrous oxide measurements. *Biogeosciences*, *15*(19), 5891–5907. https://doi.org/10.5194/bg-15-5891-2018

Yamamoto, S., Alcauskas, J. B., & Crozier, T. E. (1976). Solubility of methane in distilled water and seawater. *Journal of Chemical & Engineering Data*, *21*(1), 78–80. https://doi.org/10.1021/je60068a029

Yamamoto-Kawai, M., McLaughlin, F. A., Carmack, E. C., Nishino, S., Shimada, K., & Kurita, N. (2009). Surface freshening of the Canada Basin, 2003-2007: River runoff versus sea ice meltwater. *Journal of Geophysical Research: Oceans*, *114*(4), 2003–2007. https://doi.org/10.1029/2008JC005000

Zhou, J., Delille, B., Eicken, H., Vancoppenolle, M., Brabant, F., Carnat, G., et al. (2013). Physical and biogeochemical properties in landfast sea ice (Barrow, Alaska): Insights on brine and gas dynamics across seasons. *Journal of Geophysical Research: Oceans*, *118*(6), 3172–3189. https://doi.org/10.1002/jgrc.20232

Zona, D., Gioli, B., Commane, R., Lindaas, J., Wofsy, S. C., Miller, C. E., et al. (2016). Cold season emissions dominate the Arctic tundra methane budget. *Proceedings of the National Academy of Sciences of the United States of America*, *113*(1), 40–45. https://doi.org/10.1073/pnas.1516017113

Geophysical Research Letters

Supporting information for

River inflow dominates methane emissions in an Arctic coastal system

Cara C. Manning[1,*], Victoria L. Preston[2,3], Samantha F. Jones[4], Anna P.M. Michel[2,*], David P. Nicholson[5,*], Patrick J. Duke[4,6], Mohamed M. M. Ahmed[4], Kevin Manganini[2], Brent G.T. Else[4,], and Philippe D. Tortell[1,7]

1. Department of Earth, Ocean and Atmospheric Sciences, University of British Columbia, Vancouver, BC, Canada
2. Applied Ocean Physics and Engineering Department, Woods Hole, MA, USA
3. Department of Aeronautics and Astronautics, Massachusetts Institute of Technology, Cambridge, MA, USA
4. Department of Geography, University of Calgary, Calgary, AB, Canada
5. Marine Chemistry and Geochemistry Department, Woods Hole Oceanographic Institution, Woods Hole, MA, USA
6. Now at School of Earth and Ocean Sciences, University of Victoria, Victoria, BC, Canada
7. Department of Botany, University of British Columbia, Vancouver, BC, Canada

Corresponding authors: Cara C. Manning (cmanning@alum.mit.edu), Anna Michel (amichel@whoi.edu), David Nicholson (dnicholson@whoi.edu)

https://doi.org/10.1029/2020GL087669

Contents of this file

Introduction

The Supporting Information contains the methods section (Text S1), a description of the N_2O data (Text S2), a description of the model for calculating the CH_4 budget for the estuary (Text S3) and nine extended figures.

Text S1. Methods

Site description

Cambridge Bay (69°07'N, 105°03'W) is a small hamlet located along the south-eastern coast of Victoria Island in the Kitikmeot Region of Nunavut, Canda (Figure 1). The island is classified as part of the North American High Arctic with sedge-moss-meadow tundra and polar semi-desert (Bliss, 1981). Freshwater Creek is the most influential riverine source to Cambridge Bay, and receives discharge from Greiner Lake. A much smaller river also contributes to Cambridge Bay, and an embayment fed by this river is located northwest of the mouth of Freshwater Creek. The lake, river, and bay experience a yearly freeze-thaw cycle. The estuary freezes to ~1.5 m thick by late spring and river discharge begins in June (Figure 4 and Figure S8).

The study site is shown in Figure 1a. The ChemYak vehicle was primarily deployed in open (de-iced) regions of Cambridge Bay harbor and up to the mouth of Freshwater Creek where it became too shallow to drive the vehicle. Discrete sampling locations for the time series were located in the harbor, Freshwater Creek, and in Greiner Lake. Manual sampling locations during the course of ChemYak in situ work were in open waters and a GPS waypoint was used to flag locations.

Manual sample collection

At station B1 (69.107556 ^{o}N, 105.059667 ^{o}W), in the middle of Cambridge Bay, under-ice measurements were collected by augering a 10-inch diameter hole into the ice and open water measurements were collected by boat (~5 m long skiff). A RBR Concerto CTD was attached to a rope and lowered by hand to ~70 m, near the maximum depth. Subsequently, 1.2 L Niskin 1010 model water sampling bottles were lowered on a rope and closed at the desired sampling depths. Samples from Freshwater Creek (69.12975 ^{o}N, 104.99459 ^{o}W) were collected using a battery-powered submersible pump (Waterra Cyclone and Mini-Typhoon models were used). River temperature and salinity was measured using the RBR Concerto CTD in 2017 and a YSI ProDSS in 2018.

In ice-covered conditions, all water depths were determined relative to the top of the ice (the water surface after infilling the augered hole), rather than relative to the bottom of the ice, as the ice thickness was not measured.

Water samples for measurement of CH_4/N_2O concentration and dissolved inorganic carbon/total alkalinity (DIC/TA) were collected in 60 mL and 125 mL borosilicate serum vials, respectively. Both sample types were preserved with 0.1 mL of a saturated solution of mercuric chloride, and sealed with chlorobutyl-isoprene rubber stoppers and aluminum caps, taking care to not entrain bubbles. Samples were collected for water stable isotopic composition measurements in 2 mL glass vials with screw tops and septa. In Cambridge Bay estuary, all samples were unfiltered. At

Freshwater Creek, samples for water isotopic measurement were filtered with an in-line 0.45 µm filter (Whatman Polycap 75 GW capsule with polyethersulfone membrane) to remove particulate material, whereas CH_4/N_2O samples were left unfiltered.

Manual sample analysis

CH_4 and N_2O concentrations were determined using an automated purge and trap system coupled to a gas chromatograph-mass spectrometer (Shimadzu GCMS-QP2010) at the University of British Columbia following a published method (Capelle et al., 2015). Standard curves were prepared using a Praxair certified gas standard tank (±5% accuracy for CH_4 and N_2O) and air-equilibrated water samples were run daily to verify the accuracy of the system. The laboratory has been involved in international intercalibration exercises for oceanic CH_4 and N_2O measurements (Wilson et al., 2018). Duplicate samples were collected and duplicates with poor precision, as well as samples with clear evidence of air contamination were eliminated from the data set. For samples collected and analyzed in 2018, the expected air-equilibrated N_2O concentrations were on average 11% higher than the measured concentrations (measured N_2O concentration of 8.30± 0.49 nM N_2O, compared to the expected value of 9.23 nM). To correct the dataset, the measured N_2O concentrations of all samples analyzed during this period were increased by 11% to match the offset observed for the air-equilibrated water samples.

Dissolved inorganic carbon (DIC) concentrations were determined via acid extraction by quantifying the released CO_2 using an infrared gas analyzer (AIRICA and LICOR-7000). Total alkalinity (TA) was measured by modified Gran titration (Anderson et al., 1999) using a semi-automated open-cell titration system (AS-ALK2 Apollo SciTech) (Cai et al., 2010). All measurements were calibrated against certified reference materials (provided by A.G. Dickson from Scripps Institute of Oceanography) with a standard bottle precision of ±2.2 µmol/kg. pCO_2 values were calculated in CO2SYS (Pierrot et al., 2006) from the measured DIC and TA at in situ temperature, salinity, and pressure using published inorganic carbon dissociation constants for estuarine waters (Millero, 2010), bisulfate ion acidity constant (Dickson, 1990) and boron to chlorinity ratio (Lee et al., 2010).

Water isotope concentrations were determined using an integrated off-axis cavity absorption spectrometer (LGR Triple Liquid Water Isotope Analyzer, model 912-0032) and calibrated with VSMOW2 and SLAP2 standards, with an estimated accuracy of 0.1 and 1 permil for $\delta^{18}O$-H_2O and $\delta^{2}H$-H_2O, respectively.

Water mass analysis

Both river runoff and sea ice melt can contain elevated CH_4 (Kvenvolden et al., 1993; Stanley et al., 2016; Zhou et al., 2013). The water mass composition of near-surface samples (0.75 m depth in open water and 2 m depth under ice) at station B1 was determined using a mixing analysis. We assumed each water sample was a mixture of three endmembers (seawater, sea ice melt, and river runoff) (Macdonald et al., 1995; Yamamoto-Kawai et al., 2009) and that each endmember had unique and constant salinity (in PSS) and water isotopic composition (in ‰ versus VSMOW2-SLAP2). The following endmembers were defined for Cambridge Bay estuary: local

seawater salinity = 28.73 PSS, $\delta^{18}O\text{-}H_2O$ = -4.2 ‰, and $\delta^{2}H\text{-}H_2O$ = -32.4 ‰ (based on winter surface water measurements prior to ice melt and river discharge), local ice melt salinity = 5.16 PSS, $\delta^{18}O\text{-}H_2O$ = -2.4 ‰, and $\delta^{2}H\text{-}H_2O$ = -18.3 ‰ (based on a melted sea ice core collected at station B1), and local river runoff 0.14 PSS, $\delta^{18}O\text{-}H_2O$ = -18.5‰, and $\delta^{2}H\text{-}H_2O$ = -147.9 ‰ (based on average river water measurements in June and August). Some samples with salinity >28.5 PSS were assumed to be 100% seawater and were not analyzed for water isotopic composition.

During the melt period in June-July, near-surface samples at station B1 contained variable fractions of river water (from 0 to 85%). On some under-ice sampling dates (e.g., 24 June 2017), the high-resolution CTD profile showed that the mixed layer depth was <2 m and therefore the near-surface sample collected in a Niskin bottle centered at 2 m depth likely did not solely reflect the mixed layer composition. Additionally, tidal and wind-driven current variations may have affected the distribution of the river plume. Nevertheless, the general pattern that we observed confirmed that elevated CH_4 measurements were associated with river discharge, as all measurements of elevated CH_4 at station B1 were associated with some fraction of river discharge. Furthermore, all under-ice samples containing at least 5% river runoff contained >100 nM CH_4 and two under-ice samples with >100 nM CH_4 contained 0% sea ice melt (Figure S2). These results confirm that river discharge is the source of the elevated CH_4. All water samples collected deeper than 2 m contained <12 nM CH_4 and had salinity ≥28.5 PSS indicating they contained >99% seawater and confirming that the river inflow is constrained to a shallow surface layer, facilitating rapid ventilation once ice cover retreats.

ChemYak in situ measurements

The ChemYak is a remotely operated robotic kayak developed by Woods Hole Oceanographic Institution (WHOI) for in situ greenhouse gas measurements. The vehicle's chassis is a Mokai gas-powered air-jet propulsion kayak with servo-driven controls. A PixHawk autopilot and wireless radio network was used to remotely operate the vehicle during the field campaign. The ChemYak carried a suite of instruments including: RBR Concerto CTD, Los Gatos Research (LGR) Dissolved Gas Extraction Unit (DGEU), LGR Greenhouse Gas Analyzer (GGA), and Air-Marine 200WX Weather Station. Every instrument was programmed to take and log measurements at a frequency of 1 Hz.

The DGEU equilibrates gases through a Liqui-Cel G420 2.5 X 8 membrane contactor with a total membrane surface of 1.4 m^2 and gas volume of 150 mL and pumps water at a rate of 420 std cc min^{-1}. The GGA is designed to be field portable (15 kg, 60 W) and has a measurement range of 1-20,000 ppm for CO_2 and 0-10% for CH_4 with precision at 1Hz of < 300 ppb and < 2 ppb for each gas, respectively. The DGEU draws water in and extracts an air sample which is subsequently pumped to the GGA for content analysis (the calibration of the GGA is discussed in the following section). The inlet to the DGEU, as well as the CTD, are connected to a 10m profiling winch attached to the back of the ChemYak in order to pull water samples from throughout the upper-layer of the water column.

The ChemYak traveled an average of 11±2 km per day from 28 June through 2 July and collected >75,000 observations that are reported in this study. Observations were typically collected between 15:00-22:00 UTC.

ChemYak data analysis

Measurements collected by the ChemYak were first processed by hand to remove anomalous measurements which were typically seen at the beginning of logging and the end of logging during which the vehicle was taken in and out of the water, respectively. Data from the CTD, GGA, and Weather Station were logged on separate computers, which requires a time-based interpolation procedure in order to compare the instruments directly. The Weather Station provides the GPS coordinates for each sample, and this timestamp is used. The CTD data and GGA data are then linearly cast to the timestamp of the Weather Station to create a single dataset where each entry is considered a sample measurement and contains a time, geolocation, and set of instrument observations.

The DGEU does not perfectly extract all CH_4 and CO_2 from a water sample, and so we apply an extraction efficiency correction (Nicholson et al., 2018) by inspection of results from physical bottle samples collected contemporary to the field campaign with the ChemYak (Figure S3). The bottle samples are reported in molar and atmospheric quantities for CH_4 and CO_2 respectively. ChemYak observations, were converted from partial pressure units using CTD data and established temperature and salinity dependent gas solubilities (Wiesenburg & Guinasso, 1979; Yamamoto et al., 1976). For calibration of the CO_2 sensor, dissolved inorganic carbon (DIC) and total alkalinity (TA) were measured on bottle samples and the results were converted to pCO_2 (see *Manual sample analysis*). Uncertainty in the DIC, TA, salinity and temperature measurements, as well as uncertainty in the carbonate equilibrium constants for Arctic estuarine waters, all contribute uncertainty to the calculated pCO_2 values.

To compare with bottle samples, we filter ChemYak measurements by day the sample was taken, depth proximity (±0.38 m), and geographic proximity (within 50 m radius). We then select an extraction efficiency that corresponds to a one-to-one mapping (with no offset) between bottle samples and the average of the matching ChemYak observations. As shown in Figure S3, we apply an empirical extraction efficiency of 5.09% for CH_4 (r^2=0.842) and of 50.5% (r^2=0.717) for CO_2. One bottle sample was eliminated from the calibration as the temperature/salinity profiles indicated the Niskin sampling bottle was closed in the middle of the pycnocline where there is a sharp gradient in gas concentrations, and this sample showed very poor agreement between the bottle sample and GGA. The difference in extraction efficiency occurs as a consequence of the differences in solubility characteristics between CH_4 and CO_2.

Text S2. N_2O data

N_2O concentrations at station B1 and Freshwater Creek were close to equilibrium and displayed limited seasonal variability (Figure S1). During open water conditions in Cambridge Bay, N_2O was typically undersaturated or close to equilibrium in near-surface waters. Anoxic conditions in the sediments and water column that promote CH_4 accumulation may simultaneously drive N_2O consumption via denitrification (Naqvi et al., 2010). These conditions contrast with the lower-

and mid-latitudes where rivers and estuaries are typically considered significant N_2O sources (Seitzinger & Kroeze, 1998; Seitzinger et al., 2000). These N_2O data are provided as a supplement to the paper.

Text S3. Model for estimating CH_4 distributions and transport

Model mass balance

We developed a geochemical box model to quantify the CH_4 budget for Cambridge Bay. Model code is provided as a supplement to the paper (Manning & Preston, 2020). The estuary model domain has a volume of 5 x 2 x 10^6 m^3 (5 x 10^6 m^2 surface area and a 2 m deep mixed layer) and is shown in Figure S7. The model time-step is hourly and the domain is divided into 10 boxes (reducing the time step and box size further had a negligible impact on model output).

The model assumes conservation of water volume in each well-mixed box. In each box the volume balance at each time step is:

$V_{riv} + V_{ice} + V_{out} = 0$

where V_{riv} is the volume added from river discharge, V_{ice} is the volume added from ice melt, V_{out} is the lateral volume transferred to the adjacent box (moving toward the coastal ocean). Positive values add volume to the box. The model does not include the effects of vertical mixing and/or vertical advection, as the rate of vertical mixing coefficient is unconstrained for this system and likely inhibited by the strong vertical salinity stratification.

In the rest of the boxes, the mass balance at each time step is:

$V_{ice} + V_{out} + V_{in} = 0$

where V_{in} is the volume received laterally from the adjacent box (closer to the river) and V_{out} is the volume transferred laterally to the adjacent box (farther from the river).

For each box, at each time-step *t* the $[CH_4]$ is calculated as

$[CH_4]_{t+1} = ([CH_4]_t V_{box} + F_{riv,t} + F_{ice,t} + F_{gasex,t} + F_{in,t} + F_{out,t} + F_{ox,t}) / V_{box}$

where V_{box} is the box volume (m^3), $[CH_4]$ is the dissolved concentration in the box (mol m^{-3}) and *F* is the flux (in mol m^{-3} $timestep^{-1}$). Specifically, for box *n*, the flux from river discharge is:

$F_{riv,t} = V_{riv,t}[CH_4]_{riv,n,t}$

and V_{riv} = 0 for every box except for the first box adjacent to the river.

The flux from ice melt is

$F_{ice,t} = V_{ice,t}\,[CH_4]_{ice,n,t}$

The lateral flux in to box *n* from the adjacent box (*n-1*) is

$F_{in,t} = (V_{riv,t} + V_{ice,t})\,[CH_4]_{n-1,t-1}$

and F_{in} is 0 for box *n*=1.

The lateral flux out from box *n* to the adjacent box (*n+1*) is

$F_{out,t} = -(V_{riv,t} + V_{ic,te})\,[CH_4]_{n,t}$

The flux due to gas exchange is
$F_{ge,t} = k_{CH4,t} ([CH_4]_{eq,t} - [CH_4]_{n,t}) V_{box} dt$
where k_{CH4} is the gas transfer velocity for CH_4 (m d^{-1}) (Wanninkhof, 2014), $[CH_4]_{eq}$ is the equilibrium concentration(Wiesenburg & Guinasso, 1979) (mol m^{-3}) and dt is the timestep (d).

The flux due to microbial oxidation is
$F_{ox,t} = -k_{ox,t} [CH_4]_t V_{box} dt$
where $k_{ox,t}$ is the first order oxidation rate constant (d^{-1}). Because oxidation rates were not measured, the model was run using a range of oxidation rate constants (0, 0.01 and 0.1 d^{-1}) to investigate the potential range of impacts of microbial oxidation on the CH_4 budget (Figure 4 and S9).

Calculation of flux due to gas exchange alone
To estimate the expected gas concentration decrease for an isolated box unaffected by river inflow, we used a simplified model where
$[CH_4]_{t+1} = ([CH_4]_t V_{box} + F_{gasex,t}) / V_{box}$

Model data sources
To estimate V_{riv}, the river discharge volume flux, we used river discharge records in Freshwater Creek from 1970 to 2016 extracted from the Environment and Climate Change Canada Historical Hydrometric Data website (2019) on 10 Jan 2019 (station 10TF001) as well as preliminary discharge data from 2018 provided by A. Pippy of Environment Canada (Figure 4a). Peak discharge typically occurs in late June-early July and mean annual discharge from 1970-2016 was $1.4 \pm 0.7 \times 10^8$ m^3 (14 times the volume of the model domain). Unfortunately, the river discharge meter malfunctioned in early 2018 and the first discharge measurement for 2018 was made on 2 July 2018, slightly after the annual peak. We used the average daily discharge from 1970 to 2016 in the model, which appeared very similar to the 2018 discharge data from 2 July onward (Figure 4a).

Calculation of the gas transfer velocity, k_{CH4} requires estimates of wind speed and ice coverage. For wind speed, we used records from the Cambridge Bay airport for 2018, station WMO71288, available at http://climate.weather.gc.ca (Environment and Climate Change Canada Historical Database, 2019).

To model the volume flux of ice and the fractional ice coverage, we used ice thickness records collected via an ice draft profiler (upward-facing sonar) installed on a cabled observatory at the Ocean Networks Canada (ONC) site in Cambridge Bay estuary (69.1133 ^oN, 105.060 ^oW, Figure 1a). Corrected ice draft data from 1 January to 31 December 2018 (sensor ID 21593, device ID 24049) was used (Ocean Networks Canada Data Archive, 2019); Figure S8). These records show that the ice above the ONC sensor was ~1.43 m thick on 10 June and following 10 June, the ice thickness steadily decreased until the water became ice-free between 7-10 July. Satellite true color (corrected reflectance) images collected with Terra MODIS and Aqua MODIS and accessed using the NASA Worldview application (https://worldview.earthdata.nasa.gov/) indicated that the majority of the estuary was ice-covered on 6 July that the estuary became entirely ice free

between 7-9 July, and that the coastal ocean adjacent to the estuary became ice free around 25 July. We assumed that the model boxes closest to Freshwater Creek (Region 1, 1 km^2) became ice free on 25 June (just prior to the beginning of the ChemYak measurement campaign), the remainder of the estuary (Region 2, 4 km^2) became ice-free on 8 July, and the adjacent coastal ocean (Region 3, 60 km^2) became ice-free on 20 July. Region 1 is approximately equivalent to the 1 km^2 region that was sampled with the ChemYak from 28 June-2 July. For Region 2, we used the modeled ice thickness record based on the ONC data. For Region 1, we shifted the modeled ice thickness record in time so the melt began 13 days earlier and the station became ice free 13 days earlier, and likewise the Region 3 modeled ice thickness record was shifted 12 days later.

At each time step, each box has either 100% ice cover or 0% ice cover. For 100% ice cover, we assume there is no gas exchange flux ($k_{CH4} = 0$) (Butterworth & Miller, 2016), and for 0% ice cover, we use the gas exchange parameterization of Wanninkhof (2014). The west arm is not included in the model domain because the sea ice melt pattern in the estuary suggests the dominant flowpath for river discharge is along the east arm and through the central estuary toward the coastal ocean (Figure 1). Increasing the Region 2 domain to include the west arm would increase the total CH_4 emissions from Cambridge Bay estuary.

The value of $[CH_4]_{riv}$ is modeled using a linear interpolation on the Freshwater Creek data to match the model time steps, and the initial $[CH_4]$ in each box in the estuary is assumed to be 6 nM (typical wintertime under-ice concentration). $[CH_4]_{eq}$ is calculated using the observed salinity and temperature at station B1 (interpolated to match the model time steps) and assuming an atmospheric CH_4 concentration of 1851 ppb (mean global value for June-July 2018). $[CH_4]_{ice}$ was not measured and is assumed to be 6 nM (the typical wintertime under-ice concentration). Because the total river discharge volume is 200 times greater than the ice melt volume (V_{ice} = 7.1 x 10^5 m^3 and V_{riv} = 1.4 x 10^8 m^3), the model results are relatively insensitive to the value of $[CH_4]_{ice}$. For example, using $[CH_4]_{ice}$ = 6 nM the total annual CH_4 input from ice (cumulative F_{ice}) is 0.6 kg, and using $[CH_4]_{ice}$ = 100 nM the cumulative F_{ice} is 10 kg, compared to the cumulative F_{riv} of 803 kg.

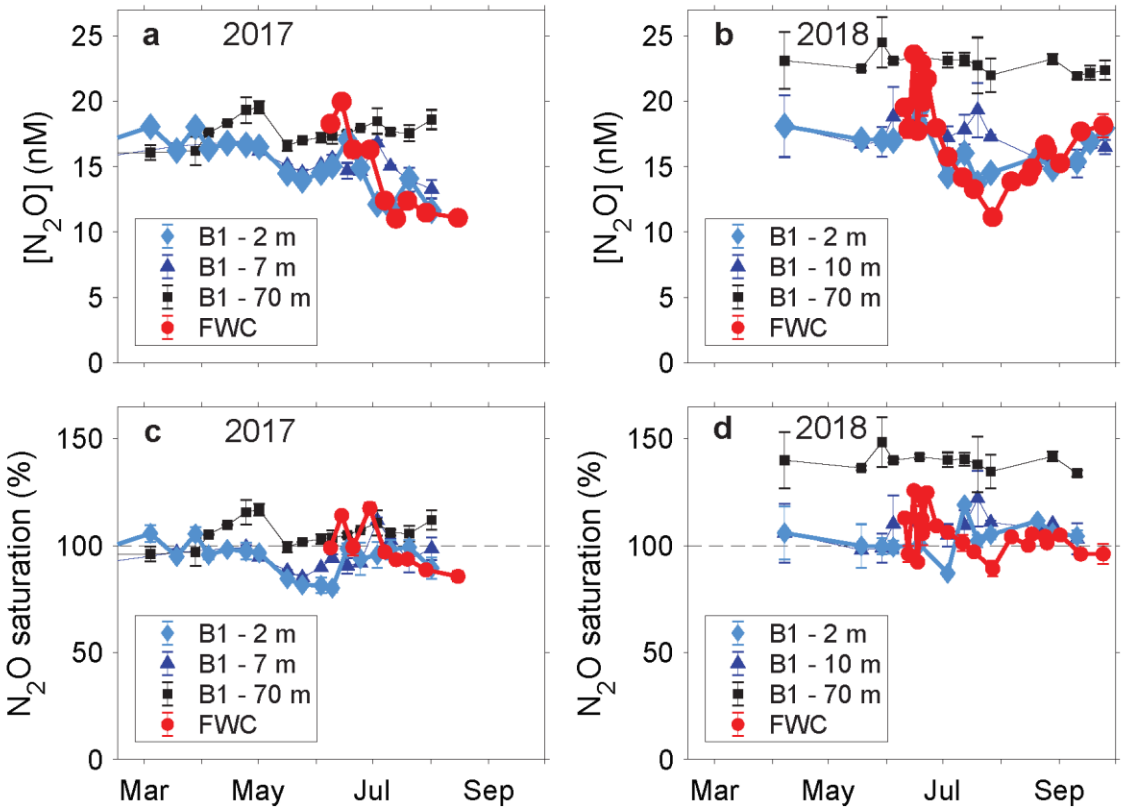

Figure S1. N_2O time-series from 2017 and 2018. N_2O concentration (**a-b**) and saturation (**c-d**) calculated using the in situ temperature and salinity and a dry atmospheric N_2O concentration of 329 ppb (Weiss & Price, 1980). Dashed line indicates atmospheric equilibrium. Samples were collected in Cambridge Bay harbour (station B1, blue and black lines) and Freshwater Creek (FWC, red line).

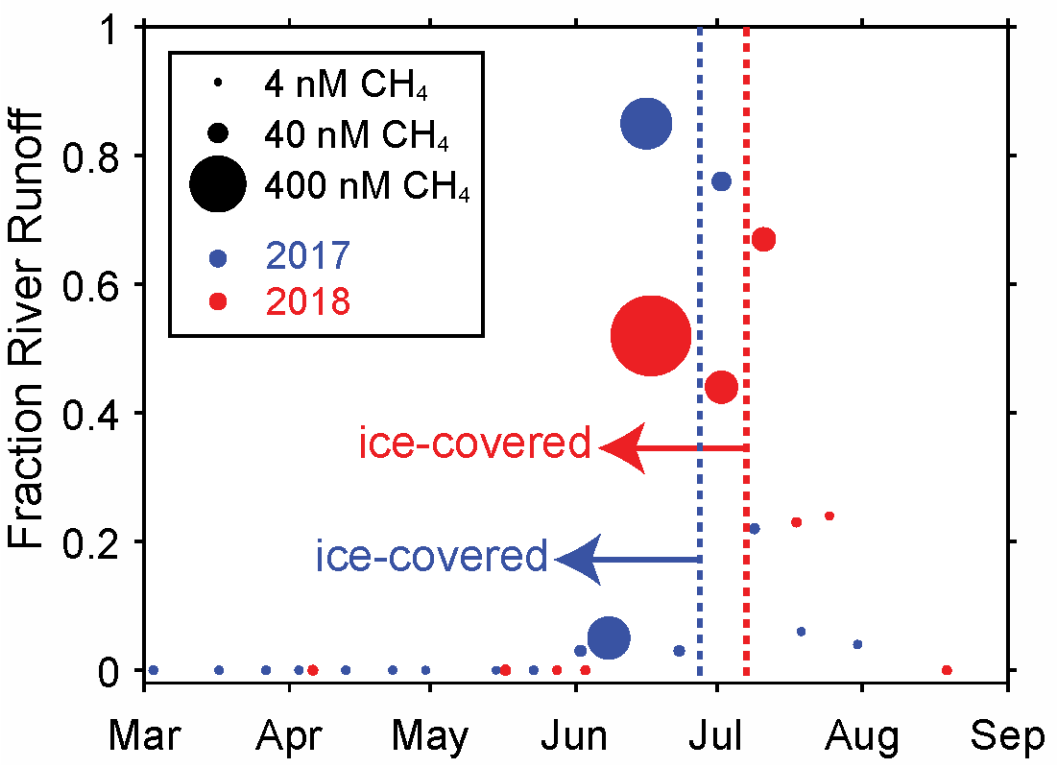

Figure S2. Water mass analysis for near-surface samples (0.75-2 m depth) at station B1. Blue symbols represent 2017 and red symbols represent 2018. Dashed lines show the timing of open water at station B1 in 2017 (blue) and 2018 (red). Highest CH_4 concentrations and highest fractions of river runoff were observed just prior to and just after ice melt. All samples with salinity > 28.5 PSS were assumed to be 100% seawater (which was assigned a salinity endmember of 28.73 PSS).

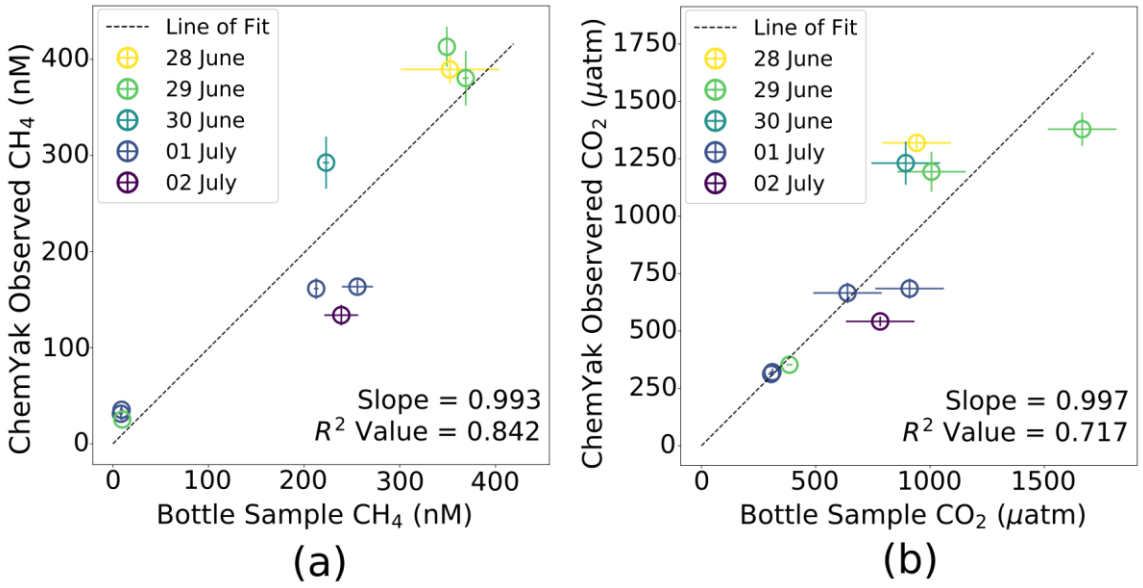

Figure S3. Calibration results for ChemYak greenhouse gas analyzer. Comparison of gas concentration measurements from discrete bottle samples and ChemYak observations. Raw measurements from the ChemYak greenhouse gas analyzer (GGA) are reported in ppm, and using simultaneous salinity and temperature measurements, we make a gas-unit conversion to molar and atmospheric quantities for comparison with bottle samples. To correct for incomplete gas extraction, we apply a gas extraction efficiency coefficient that is empirically determined by comparing ChemYak observations with paired bottle samples. In the plots above, ChemYak observations of CH_4 and CO_2 are calculated using an extraction efficiency of 5.09% (r^2=0.842) and 50.5% (r^2 = 0.717), respectively. ChemYak measurements are representative of the mean (location) and standard deviation (errorbar) of all data filtered by location (<50 m radius), depth (±0.38m), and day, as recorded for the bottle sample.

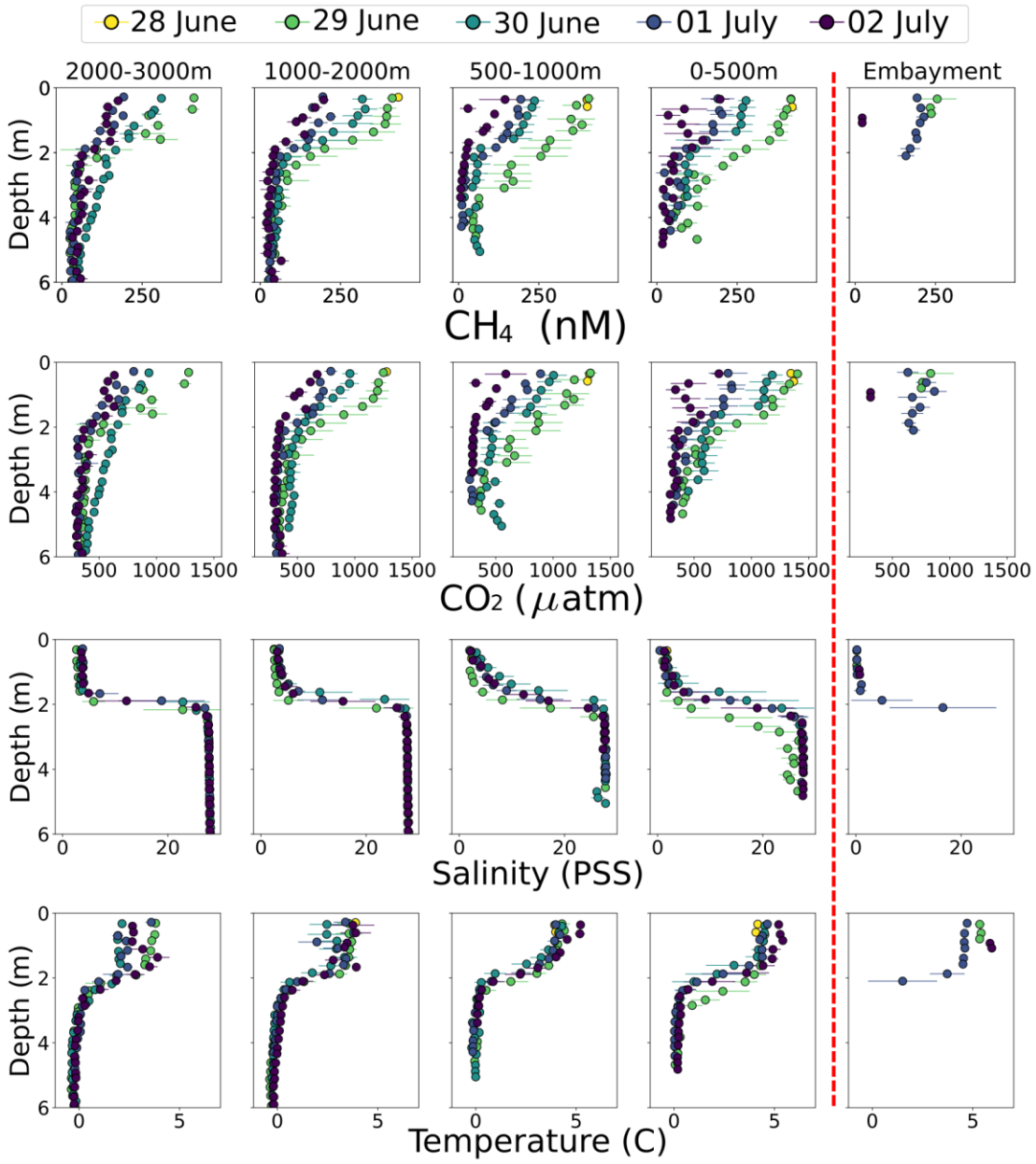

Figure S4. Depth versus value binned by distance from Freshwater Creek. To observe regional variation in CH_4, CO_2, salinity and temperature between the mouth of Freshwater Creek (0-500m) the embayment to the northeast, and the ice edge downstream to the southwest (>500 m), we bin the observations of the ChemYak by day (color), depth (0.25 m), and distance. Circles and lines represent the mean and standard deviation for each bin. The embayment water was generally warm and fresh, with uniformly low CH_4 and CO_2 concentrations in the three days it was observed (29 June, 1 July, and 2 July). Generally the stratification of the water column, as observed by salinity and temperature, became less pronounced as distance from the mouth of Freshwater Creek decreased, indicating more vertical mixing. Elevated CH_4 and CO_2 was evident below 2 m depth towards the ice edge on 30 June compared to other days, likely due to increased wind speeds.

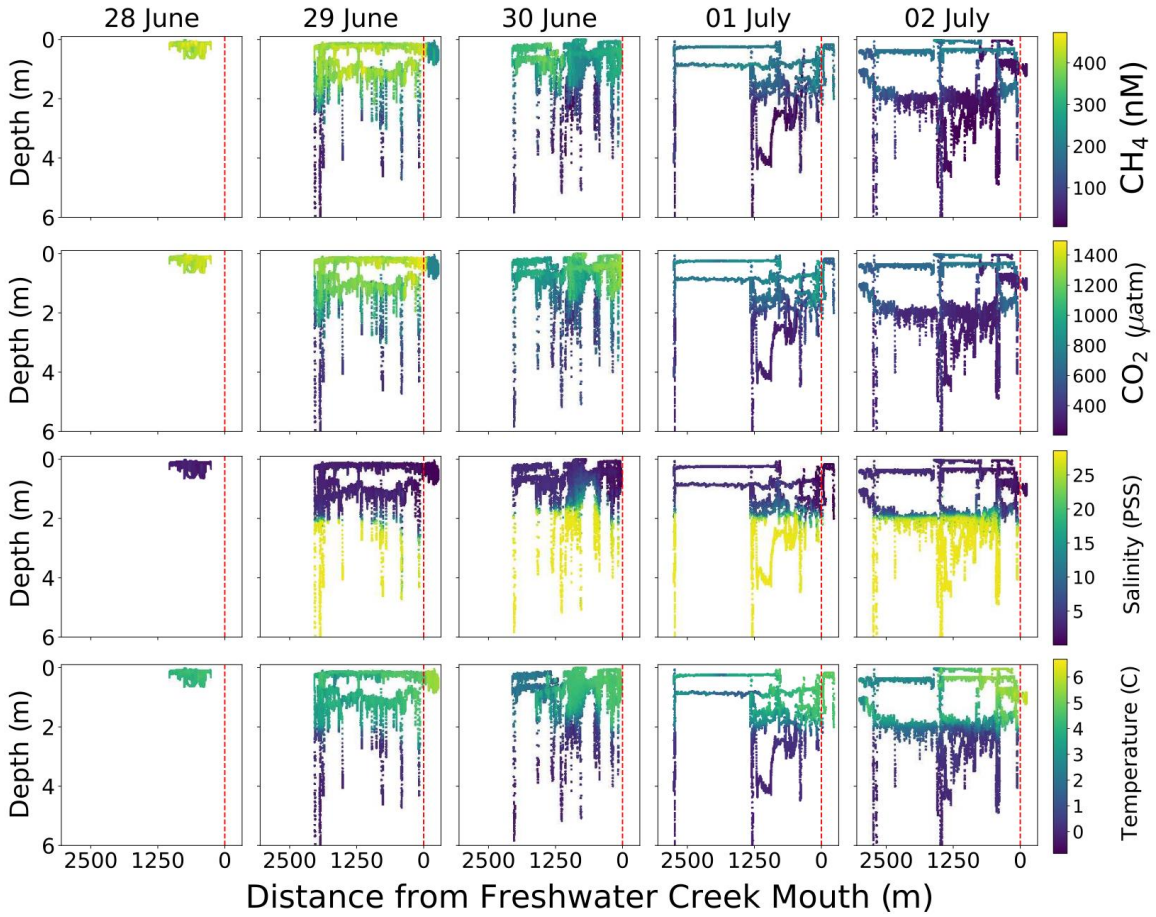

Figure S5. Complete depth-distance plots. See Figure 2a for the map used to calculate distance from Freshwater Creek mouth. The data shown for 29 June and 2 July is equivalent to Figure 2 b-g.

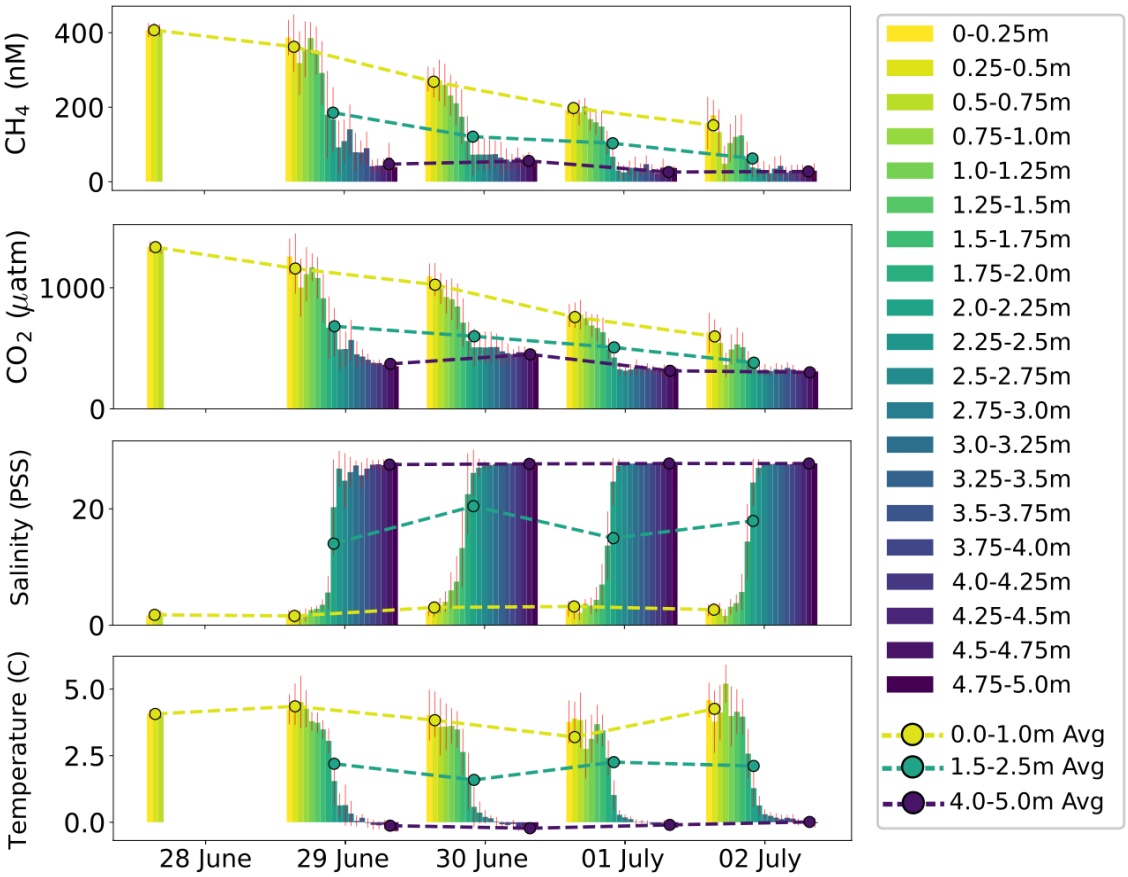

Figure S6. ChemYak bar graphs. Bar graphs with error bars showing CH_4, CO_2, salinity, and temperature, colored by depth binned in 0.25 m intervals. Trend lines are added to show the average value of measurements in the surface layer (top 1 m), the pycnocline (1.5-2.5m), and below the pycnocline (4-5 m). On 30 June, elevated wind briefly disturbed the pycnocline leading to vertical mixing, as evidenced by elevated CO_2 and CH_4 levels below the mixed layer, and elevated Salinity in the surface layer. Both CH_4 and CO_2 decreased substantially in the surface layer over the 5 day measurement period.

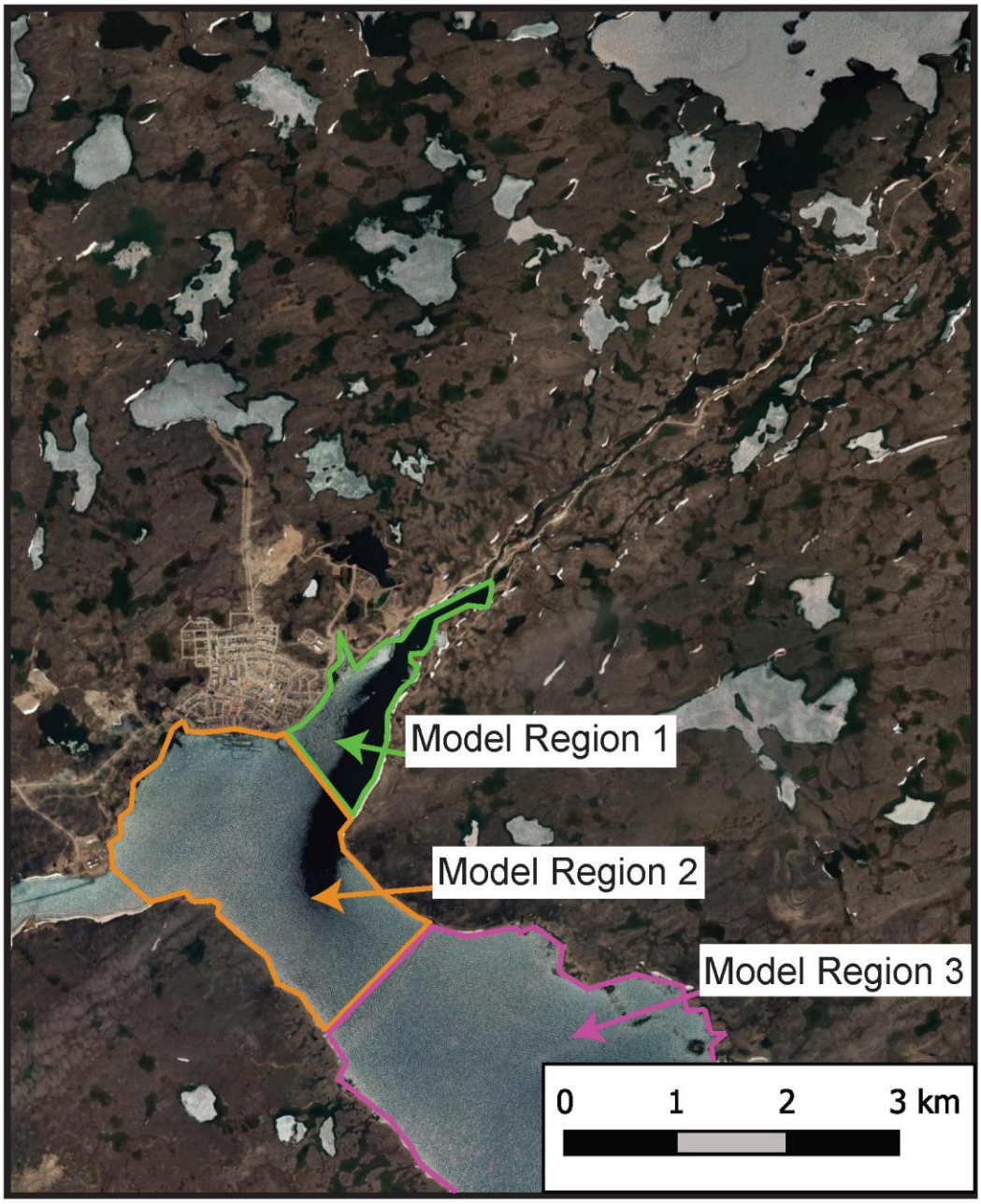

Figure S7. Model domain. Map showing model Model Regions 1, 2, and 3 (see Text S1). The satellite image was collected on 21 June 2017 and was obtained from Google, DigitalGlobe

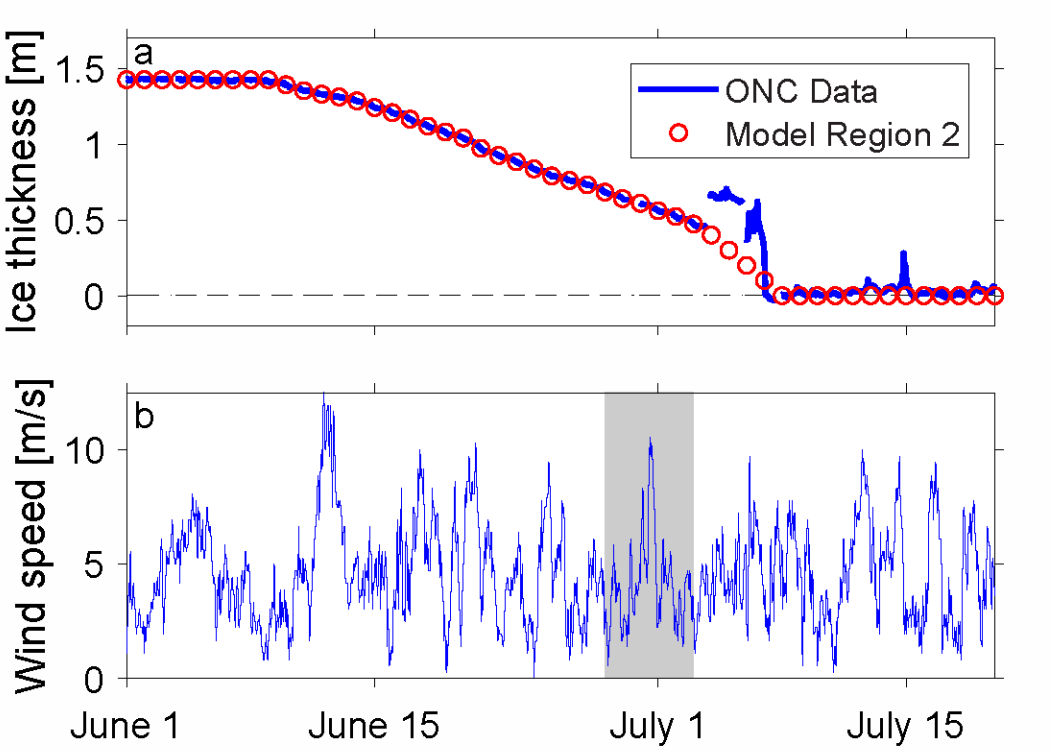

Figure S8. Ice thickness and wind speed data. **a** Ocean Networks Canada ice thickness data (blue line) and modeled daily values (red circles) used to generate model shown in Figure 4. **b** Wind speed records from Cambridge Bay airport. The ChemYak sampling period is shown with a shaded gray bar.

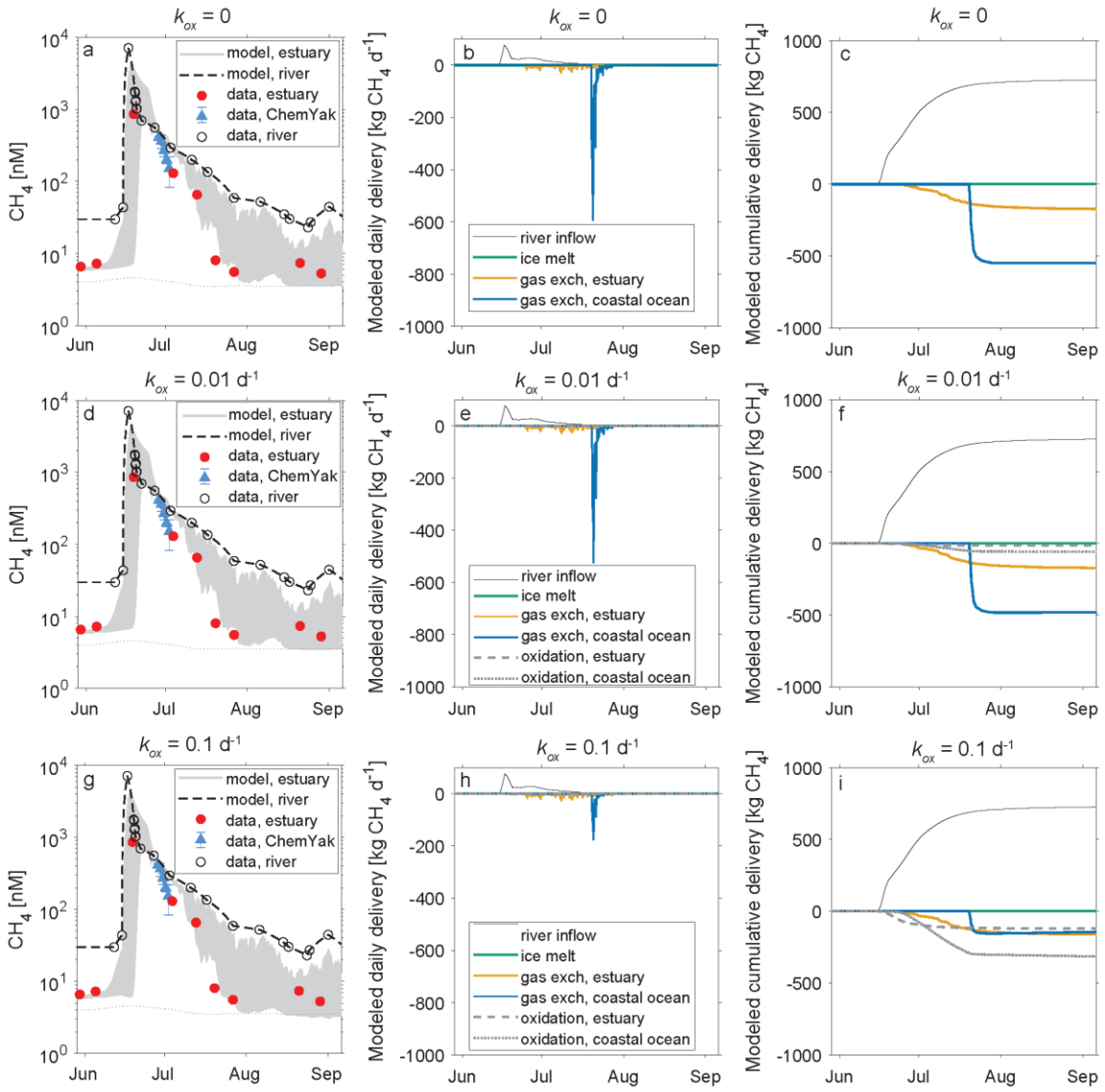

Figure S9. Model results with varying methane oxidation rate constants: 0 (**a-c**),0.01 d^{-1} (**d-f**), and 0.1 d^{-1} (**g-i**). Note that Figure S9 a-c is equivalent to Figure 4 b-d.